THESIS FOR THE DEGREE OF DOCTOR OF PHILOSOPHY

Electromechanical Phenomena in Superconducting and Normal Nanostructures

MILTON EDUARDO PEÑA AZA

GÖTEBORGS UNIVERSITET

Department of Physics
University of Gothenburg
SE-412 96 Göteborg, Sweden 2013

Electromechanical Phenomena in Superconducting and Normal Nanostructures
MILTON EDUARDO PEÑA AZA
ISBN: 978-91-628-8699-8
Electronic version available at:
http://hdl.handle.net/2077/32677

Doktorsavhandling vid Göteborgs Universitet

Condensed Matter Theory Group
Department of Physics
University of Gothenburg
SE-412 96 Göteborg
Sweden
Telephone +46 (0)31 786 0000

Typeset in LaTeX

Figures created using MATLAB, GIMP, POV-Ray, MATHEMATICA and Paint.
The suspended carbon nanotubes illustrations were created by Yury A. Tarakanov, Gustav Sonne and Tomasz Antosiewicz. The time evolution of voltage-driven Andreev levels image was done by Gustav Sonne.

Printed by Kompendiet
Göteborg, Sweden 2013

Electromechanical Phenomena in Superconducting and Normal Nanostructures

MILTON EDUARDO PEÑA AZA
Condensed Matter Theory
Department of Physics
University of Gothenburg

ABSTRACT

This thesis summarizes a series of theoretical studies on the electromechanical properties of nanostructures made of superconducting and/or metallic elements. The first part of the work is devoted to the analysis of the interactions between the electronic and mechanical degrees of freedom in suspended nanowires. In particular, a metallic carbon nanotube fixed between two superconducting leads and acting as a superconducting weak link is considered. This system is denoted as a *nanoelectromechanical Josephson junction*. If biased by a dc voltage, such a nanodevice possesses the ability to self-cool through the transfer of energy from the flexural vibrations of the suspended nanowire to voltage-driven Andreev states and then to quasiparticle electronic states in the superconducting leads. The electromechanical coupling required to accomplish the energy transfer process can be attained by applying an external magnetic field. It gives rise to a Lorentz force that couples displacements of the carbon nanotube to the electrical current that is carried by Andreev states.

Further investigations of the nanoelectromechanical Josephson junction extend the analysis of the first study to a case in which the system is subjected to a nonuniform magnetic field. In this case, inhomogeneity of the field causes the conducting nanoresonator to execute a whirling movement. The analysis of the time evolution of the amplitude and relative phase of the nanowire motion shows that the coupled amplitude-phase dynamics presents different regimes depending on the degree of inhomogeneity of the magnetic field: time independent, periodic, and chaotic.

The second part of the thesis describes the dynamics of a spatially symmetric shuttle-system subjected to an ac gate voltage. In this system, parametric excitation gives rise to mechanical vibrations at the resonant frequency, *i.e.*, when the frequency of the ac signal is close to the eigenfrequency of the mechanical subsystem. The parametrically excited mechanical oscillations result in a dc shuttle current in a certain direction due to spontaneous symmetry breaking, where the direction of the current is determined by the phase shift between the ac voltage and the induced mechanical oscillations.

Keywords: Nanoelectromechanical systems, nanoelectromechanical Josephson junction, metallic carbon nanotubes, ground-state cooling, chaos, parametric excitation, dc shuttle current.

Research publications

This thesis is an introduction to and summary of the work contained in the following research articles printed as appendices and referred to, by capital Roman numerals in the text, as Papers I-IV.

PAPER I

Cooling of a suspended nanowire by an ac Josephson current flow
G. Sonne, M.E. Peña-Aza, L.Y. Gorelik, R.I. Shekhter and M. Jonson
Physical Review Letters **104**, 226802 (2010).

PAPER II

Voltage-driven superconducting weak link as a refrigerator for cooling of nanomechanical vibrations
G. Sonne, M.E. Peña-Aza, R.I. Shekhter, L.Y. Gorelik and M. Jonson
Fizika Nizkikh Temperatur **36**, Nos. 10/11, 1128 (2010).

PAPER III

Dynamics of a suspended nanowire driven by an ac Josephson current in an inhomogeneous magnetic field
M.E. Peña-Aza
Physical Review E **86**, 046208 (2012).

PAPER IV

Parametric excitation of a dc shuttle current via spontaneous symmetry breaking
M.E. Peña-Aza, Alessandro Scorrano and L.Y. Gorelik
arXiv:1212.1035 (2012)
Submitted to Physical Review B.

These articles are appended at the end of the thesis.

The specific contribution by the author, M.E. Peña-Aza, to the appended papers was the following,

PAPERS I - II

I performed preliminary model calculations for the problem, optimized the numerical code in order to obtain the dc current through the system, and took part in the analysis and discussion. I also participated in the writing process of the articles.

PAPER III

I am the sole author.

PAPER IV

I performed the model calculations and numerical simulations. I took part in discussions and analysis of the results. I also participated in the writing process of the article.

TABLE OF CONTENTS

CHAPTER 1

Introduction

Recent developments in nanotechnology have made possible the design and fabrication of nanomechanical resonators with high resonance frequencies (10^6-10^9 Hz), high quality factors Q (10^3-10^5), and small masses (10^{-15}-10^{-17} kg) [1–5]. These attributes make nanoelectromechanical systems (NEMS) excellent devices for investigations in basic science and engineering. Indeed, nanoelectromechanical systems have been widely used for the exploration of the quantum world and for the development of new technological applications [6–9]. In basic research NEMS are considered promising candidates for studying the quantum limit of mechanical motion [**?**,10–13]. It is expected that the quest for the quantum regime in such devices will elucidate questions of fundamental nature in physics, for instance, the quantum-mechanical description of macroscopic objects [14–18]. In addition, mechanical systems at the quantum limit may become useful for applications in high precision measurements [19–21].

This thesis presents theoretical studies of two different nanoelectromechanical systems. The first part of the work is mainly based on the effects of electromechanical coupling in a nanodevice where an oscillating suspended nanowire forms a weak-link between two superconductors, *a nanoelectromechanical Josephson junction*. The material covered in the second part of the thesis deals with parametric effects in a nanoelectromechanical shuttle system.

Three important outcomes from our research are the possibility to cool down the flexural vibrations of the oscillating suspended nanowire, to devise a setup for studying nonlinear dynamics and chaos at the nanoscopic level and, to generate a dc current in a completely symmetric shuttle system.

Before continuing, we take a brief moment to introduce some concepts and terminology that will be used in this thesis. This is done in the following sections.

1.1 Mechanical properties of suspended nanowires

One of the main objectives of this thesis is to study how the oscillatory motion (mechanical degrees of freedom) of a suspended nanowire affects its charge transport properties (electronic degrees of freedom). Thus, it is important to understand the mechanical properties of suspended nanowires. The modal analysis of a nanomechanical resonator can be obtained from the Euler-Bernoulli formalism [22]. The geometry under consideration consists of a nanobeam clamped at the two ends as depicted in Fig. 1.1

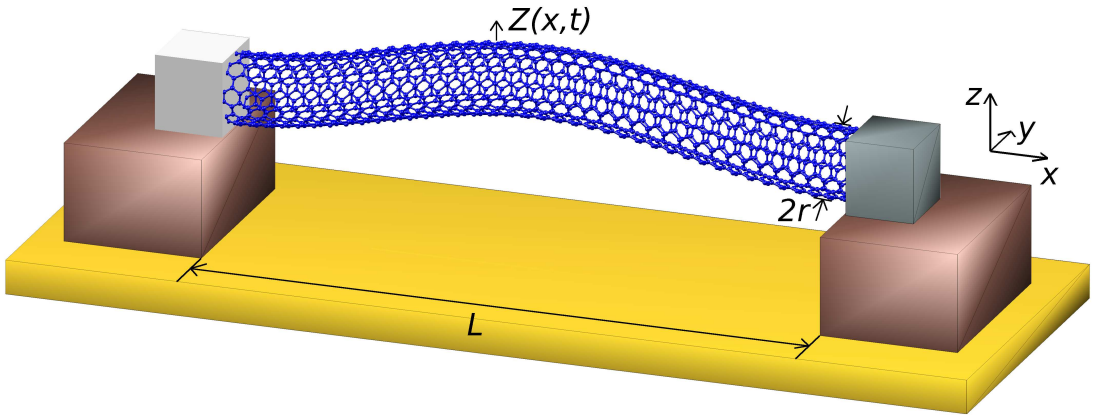

Figure 1.1: Schematic diagram of a nanomechanical oscillator. A nanowire of length L is suspended between two pillars.

The physical parameters of the nanobeam are: length L, elasticity modulus E, moment of inertia I, density ρ, and cross-sectional area A_c. For an isotropic nanobeam with a uniform cross-section, in the limit of small amplitudes, the position dependent displacement in the x-direction, $Z(x,t)$, satisfies the following differential equation

$$\rho A_c \frac{\partial^2 Z(x,t)}{\partial t^2} + EI \frac{\partial^4 Z(x,t)}{\partial x^4} = f(x,t)\,. \tag{1.1}$$

In Eq. (1.1) the first term on the left hand side comes from the inertial effect of the motion and the second one represents the stress in the beam due to deformations. On the right hand side, it is assumed that the nanobeam is under a time-varying external force $f(x,t)$. To evaluate further, the displacement of the nanotube, (in the z-direction as shown in Fig. 1.1), $Z(x,t)$ can be expanded in terms of a complete set of orthogonal functions $\psi_n(x)$

$$Z(x,t) = \sum_n \psi_n(x)\theta_n(t)\,, \tag{1.2}$$

where $\theta_n(t)$ is the time-dependent amplitude of motion and the set functions $\psi_n(x)$ are the normal modes of oscillation for the doubly-clamped beam. the index $n = 0, 1, 2, 3, \cdots$, accounts for the oscillation mode. The form of the normal modes $\psi_n(x)$ and their corresponding frequencies ω_n can be obtained by substituting Eq. (1.2) in Eq. (1.1)

$$EI \sum_n \theta_n(t) \frac{\partial^4 \psi_n(x)}{\partial x^4} + \rho A_c \sum_n \psi_n(x) \frac{\partial^2 \theta_n(t))}{\partial t^2} = f(x,t)\,. \tag{1.3}$$

Here on, the modal analysis is restricted to the homogeneous case $f(x,t) = 0$. As a consequence, Eq. (1.3) leads to the following equations

$$\frac{\partial^4 \psi_n(x)}{\partial x^4} - \beta_n^4 \psi_n(x) = 0\,, \tag{1.4}$$

$$\frac{\partial^2 \theta_n(t)}{\partial t^2} = -\beta_n^4 \frac{EI}{\rho A_c} \theta_n(t) = -\omega_n^2 \theta_n(t)\,. \tag{1.5}$$

Here, $\beta_n = (\rho A_c/EI)^{1/4}\omega_n^{1/2}$ is a constant for each mode n that depends on the geometry and the material. A general solution of Eq. (1.4) is

$$\psi_n(x) = a_n \cos(\beta_n x) + b_n \sin(\beta_n x) + c_n \cosh(\beta_n x) + d_n \cosh(\beta_n x)\,. \tag{1.6}$$

The boundary conditions for a doubly-clamped nanobeam are

$$\psi_n(0) = \psi_n(L) = \frac{\partial \psi_n(x)}{\partial x}\Big|_{x=0} = \frac{\partial \psi_n(x)}{\partial x}\Big|_{x=L} = 0\,. \tag{1.7}$$

When these boundary conditions are applied to Eq. (1.6), they imply that $a_n = -c_n$, $b_n = -d_n$

$$\psi_n(x) = a_n\big[\cos(\beta_n x) - \cosh(\beta_n x)\big] + b_n\big[\sin(\beta_n x) - \sinh(\beta_n x)\big]\,, \tag{1.8}$$

$$\frac{a_n}{b_n} = \frac{\cosh(\beta_n L) - \cos(\beta_n L)}{\sin(\beta_n L) + \sinh(\beta_n L)}\,, \tag{1.9}$$

$$\cos(\beta_n L)\cosh(\beta_n L) - 1 = 0\,. \tag{1.10}$$

The zeroes of Eq. (1.10) can be found numerically, with

$$\beta_n L \sim 4.73\,, 7.85\,, 10.99\,, 14.14\ldots \tag{1.11}$$

These values can be used for the estimation of the corresponding resonance frequency of each mode,

$$\omega_n = \beta_n^2\sqrt{\frac{EI}{\rho A_c}}\,. \tag{1.12}$$

This expression provides only an order of magnitude estimate for the frequency in real nanomechanical resonators. Vibrating systems at the nanometer scale are sensitive to mechanical stress resulting from coupling with the external environment.

1.2 The harmonic oscillator

This thesis is about nanoelectromechanical systems. Our frameworks to study NEMS are the languages of classical and quantum mechanics. It is the objective of this Section to give a short introduction to the physics of classical and quantum harmonic oscillators. Several systems can be modeled as a harmonic oscillator, *e.g.*, a mass on a spring, a pendulum or the relative motion of atoms in molecules. In Papers I - III we will consider oscillations of suspended nanowires which can also be described as harmonic oscillators. From the mathematical point of view, the classical harmonic oscillator is described by the equation

$$\frac{mv^2}{2} + \frac{kx^2}{2} = E. \tag{1.13}$$

Here, on the left-hand side of the equation, the first term corresponds to the energy that the oscillator possesses due to its motion, *i.e.*, kinetic energy. Similarly, the second term is the energy associated with the position of the object in space, *i.e.*, potential energy. On the right-hand side of the equation, E is the total energy of the system

which is a conserved quantity and can take any value. At the equilibrium position (oscillator at rest position) the energy of the oscillator is zero. In Eq. (1.13), m is the mass of the oscillator, v is its velocity, x is its deflection coordinate and k the spring constant.

The description of the quantum harmonic oscillator is different. The dynamics is described through the Schrödinger equation,

$$\hat{H}|n\rangle = \left(\frac{\hat{p}^2}{2m} + \frac{m\omega^2\hat{x}^2}{2}\right)|n\rangle = E_n|n\rangle, \tag{1.14}$$

for the energy eigenstate $|n\rangle$. In the Schrödinger equation ω is the frequency at which the object oscillates, $\hat{p}$ and $\hat{x}$ are the momentum and position operators, respectively. It turns out that the energy of the quantum harmonic oscillator can not take any value as in the classical case. Rather, the energy can take discrete values $E_n = \hbar\omega(n + 1/2)$ where $n = 0, 1, 2....$ Therefore, the energy of the quantum harmonic oscillator is quantized in multiples of the energy scale of the oscillator $\hbar\omega$.

In accordance with the above energy equation at $n = 0$ the energy of the oscillator is $\hbar\omega/2$, and we say that the oscillator is in its *ground state*. To attain the ground state the system must be cooled down to temperatures close to the absolute zero temperature. Even at zero temperature the oscillator can vibrate with an amplitude which is known as the zero-point amplitude.

1.3 Mechanical systems in the quantum regime

The position measurement of any oscillator is limited by quantum mechanics, *i.e.*, the harmonic oscillator is no longer considered a classical object when the position amplitude fluctuations of the resonator become comparable to the width of its wavefunction [23]:

$$\Delta x = \sqrt{\frac{\hbar}{2m\omega}}\,, \tag{1.15}$$

This quantity, which is the root mean square amplitude of quantum fluctuations or the zero-point amplitude, defines the **standard quantum limit** [16]. To enter the quantum regime the thermal energy, k_BT, is required to be much less than the associated mechanical energy quantum, $\hbar\omega$, *i.e.*

$$k_BT \ll \hbar\omega\,. \tag{1.16}$$

In the last equation k_B is the Boltzmann constant, $\hbar$ is the reduced Planck constant, and T is the temperature of the environment.

1.4 Superconducting weak links

A superconducting weak link is an insulating or conducting element that connects two superconductors [24]. Considering a normal metal weak link, the resulting structure is an S-N-S junction. Before describing the electronic properties of such a superconducting device a few words about superconductivity and the Josephson effect will be mentioned.

- Superconductivity is a phenomenon in which some materials expulse the magnetic field and have no electrical resistence below a critical temperature T_C [25]. Superconductivity was discovered by H. Kamerlingh Onnes in 1911 [26] and the microscopic description of the phenomenon was formulated by Bardeen, Cooper and Schrieffer (BCS-theory) in 1957 [27]. The main idea behind the theory is that an effective attractive interaction between electrons will lead the formation of Cooper pairs. These are correlated and form a quantum-mechanical condensate characterized by the order parameter $\Delta_0 \exp(i\phi)$. The magnitude of the order parameter is Δ_0 and ϕ is the superconducting phase. The ground state is separated from the excited states by an energy gap of size $2\Delta_0$.

- The Josephson effect is a phenomenon in which a non-dissipative current can flow between two weakly coupled superconductors separated by a non superconducting thin barrier or a narrow channel [28]. The current is driven by the phase difference between the two superconductors. The Josephson effect can be classified depending on whether an external voltage V is applied to the junction. In the first case, in the absence of voltage, a dc current can flow between the superconductors (dc Josephson effect). In the second case, under the effect of a constant voltage V, the current across the junction will oscillate in time at a frequency proportional to the applied voltage (ac Josephson effect).

Proceeding with the initial discussion, the electronic properties of the S-N-S Josephson junction can be understood by introducing a scattering process called *Andreev Reflection* [29, 30]. At the interface between a superconductor and a normal metal element, an electron incident from the normal part with an energy $E < \Delta$ may be reflected as a hole. In this process the incoming electron combines with a time-reversed electron below the Fermi energy and both enter the superconductor material as a Cooper pair. A hole is created in order to conserve the charge of the system and it travels in the opposite direction. Similarly, when this hole reaches the opposite S-N interface, it will be reflected as an electron and multiple electron/hole reflections will occur. Andreev reflection is an elastic process, thus all the particle reflections can constructively interfere and create two bound states: *Andreev states*. One of the most important characteristics of the Andreev bound states is the possibility to carry current [31–33]. This can be realized by noting that the Andreev scattering process is an effective electronic transport mechanism as it moves Cooper pairs between the superconductors. In the following sections the spectrum of the Andreev levels and the Josephson effect are studied in detail.

1.4.1 Andreev levels

The quantum-mechanical properties of the S-N-S junction can be determined by using the Bogoliubov-de Gennes equations for the two-component wave function Ψ [34]:

$$H\Psi = E\Psi, \qquad \Psi = \begin{pmatrix} \nu \\ \varphi \end{pmatrix} \qquad H = \begin{pmatrix} T & \Delta \\ \Delta^* & -T \end{pmatrix}, \tag{1.17}$$

where $T = -\hbar^2\nabla^2/2m - \mu$ is the kinetic energy operator and μ is the chemical potential.

In order to find the energy dependance of the Andreev states, it is assumed that the length of the superconducting weak link L is shorter than the coherence lenght in the superconductors ξ_0, *i.e.*, $L \ll \xi_0 = \hbar v_F/\Delta_0$ where v_f is the Fermi velocity. This regime corresponds to the short-junction limit where the spatial dependance of the order parameter can be described avoiding the problem of self-consistency.

Considering that the region $|x| < L/2$ corresponds to the normal metal weak link and the space $|x| > L/2$ to the superconductors, which for simplicity are assumed to be identical, *i.e.*, $\Delta_1 = \Delta_2 = \Delta_0, T_{C1} = T_{C2} = T_C$. It is assumed that the order parameter $\Delta(x)$ changes as $|\Delta(x)| = \Delta_0$ when $|x| > L/2$ and $|\Delta(x)| = 0$ when $|x| < L/2$ on the interface between the normal metal and the superconductor[1]. However, the phases of the order parameters in the superconductors may differ as $\arg\Delta(x) = \phi_1$ for the superconductor placed in the region $x < -L/2$ and $\arg\Delta(x) = \phi_2$ when $x > L/2$. Therefore, the spacial dependence of the order parameter can be approximated as [36]

$$\Delta(x) = \begin{cases} \Delta_0 \exp(i\phi_1), & \text{if } x < -L/2, \\ 0, & \text{if } |x| < L/2, \\ \Delta_0 \exp(i\phi_2), & \text{if } x > L/2. \end{cases} \tag{1.18}$$

The solution of Eq. (1.17) can be found by matching the wave functions in the different regions [36–39]. The energy spectrum depends on the scattering processes taken into consideration.

- By considering only Andreev reflections in the system, the energy spectrum as a function of the phase difference $\phi = \phi_2 - \phi_1$ between the superconductors is [36]:

$$E_\pm(\phi) = \pm\Delta_0 \cos(\phi/2)\,. \tag{1.19}$$

  This mathematical expression for the energy spectrum implies that there are two bound Andreev levels, *i.e.*, a single bound state at positive energies $E > 0$ and its mirror image at negative energies $E < 0$.

- By including Andreev reflections and electronic scattering due to impurities in the normal part, the energy espectrum is given by [37,40,41]:

$$E_\pm(\phi) = \pm\Delta_0 \sqrt{1 - D\sin^2(\phi/2)}\,. \tag{1.20}$$

  In the last equation, $D = 1 - R$, is the normal transmission coefficient. It can be noticed that the case, $D = 1$, corresponds to the clean junction, Eq.(1.19).

1.4.2 DC Josephson current

The Josephson current is calculated from the Andreev level spectrum as [40]:

$$I(\phi) = \frac{2e}{\hbar}\frac{\partial E(\phi)}{\partial \phi}\,. \tag{1.21}$$

[1] This model is known as *rigid boundary condition model*, and it is discussed in Refs [35] and [24]

For a clean junction, the bound state current can be found by direct substitution of Eq. (1.19) into Eq. (1.21) and it is,

$$\begin{aligned} I(\phi) &= \pm\frac{2e}{\hbar}\frac{\partial E(\phi)}{\partial \phi} \\ &= \mp\frac{\Delta_0 e}{\hbar}\sin(\phi/2)\,. \end{aligned} \tag{1.22}$$

The current in Eq. (1.22) is proportional to the sine of the phase difference between the superconductors. For junctions sustaining both normal and Andreev reflections, the current is given by

$$\begin{aligned} I(\phi) &= \pm\frac{2e}{\hbar}\frac{\partial E(\phi)}{\partial \phi} \\ &= \mp\frac{\Delta_0 e}{2\hbar}\frac{D\sin(\phi)}{\sqrt{1-D\sin^2(\phi/2)}}\,. \end{aligned} \tag{1.23}$$

This current is obtained by substituting Eq. (1.20) into Eq. (1.21).

1.4.3 AC Josephson effect

By applying an external voltage V between the superconductors, the superconducting phase difference ϕ is related to the bias voltage through the expression [42]:

$$\frac{d\phi}{dt} = \frac{2eV}{\hbar}\,. \tag{1.24}$$

A solution of Eq. (1.24) is:

$$\phi(t) = \frac{2eVt}{\hbar} + \phi_0\,. \tag{1.25}$$

Hence, the phase difference evolves linearly in time. In Papers I - II, it is assumed that the adiabatic condition for the phase evolution is fulfilled, *i.e*,

$$\hbar\dot{\phi} \ll \Delta_0. \tag{1.26}$$

Therefore, one can assume that the Andreev levels move adiabatically within the superconductor energy gap.

$$E_\pm(\phi) \to E_\pm(\phi(t))\,. \tag{1.27}$$

This adiabatic motion will play an important role on the research topic covered in Papers I-II.

1.4.4 Crisis and chaotic attractors

One of the research topics covered in this thesis is NEMS as dynamical systems exhibiting complex behavior. We will focus our attention on the occurrences of sudden qualitative changes of chaotic attractors as a parameter is varied. These phenomena are well known in bifurcation theory and they are denoted *crises*.

Our research in this thesis concerns chaotic attractors and their dynamics. We would like to define an attractor as a compact set with a neighborhood such that,

for almost every initial condition in this neighborhood, the limit set of the orbit as time tends to $+\infty$ is the atractor. In other words, an attractor is a set towards which a variable for a given dynamical system evolves over time in accordance with the differential equation that determines its dynamics. Thus, points that get close enough to the attractor keep close even if they are slightly disturbed.

A chaotic attractor can be thought of as a surface in the phase space of the dynamics variables, to which the system orbit is asymptotic in time and on which it wanders in a chaotic fashion. In a chaotic attractor there is a sensitive dependence on initial conditions. From the mathematical point of view a chaotic attractor is one for which typical orbits on the attractor have a positive Lyapunov exponent [43].

In this thesis we study sudden qualitative changes of chaotic dynamics (crises) and it is possible to identify different types of crises [44],

- ***Boundary or exterior crisis.*** A boundary crisis occurs when a chaotic attractor collides with an unstable periodic orbit on the basin boundary, converting the attractor into a nonattracting chaotic set and generating transient chaos. In this case, for parameter values just past the crisis point, the attractor no longer exists. Nonetheless, typical trajectories initialized in the region formerly occupied by the destroyed attractor appear to move about in this region chaotically, as before the crisis occurred, but only for a finite time after which the orbit rapidly leaves the region [45].

- ***Interior crisis.*** In the case of an interior crisis, there is a sudden increase in the size of a chaotic attractor as a parameter passes through the crisis point.

- ***Attractor merging crisis.*** In this case, for parameter values just before the crisis point, two chaotic attractors coexist, each having its own basin of attraction. As the parameter is increased, the two attractors enlarge, and at the crisis point they collide with the basin boundary separating their basins. As a consequence, the two chaotic attractors merge together to increase in size. Merging crisis can happen in systems possessing some symmetry whereby the precrisis attractors, as well as their basins, are symmetric images of each other in the phase space.

In Chapter 4 we will introduce a *nanoelectromechanical Josephson junction* in an inhomogeneous magnetic field and analyze how the dynamical bahavior of the system leads to an example of an attractor merging crisis. For a review on dynamical system, nonlinear phenomena and crises the reader is referred to Refs. [43–48].

1.4.5 Shuttle mechanism of charge transport

Some years ago, a novel form of electron transport (shuttle transport of electrons) based on the mechanical vibrations of a metallic nanoparticle coupled to two electrodes via elastic molecular links was proposed in Ref. [49]. Since then, the shuttle phenomena has been a subject of intensive experimental and theoretical research [50–55].

The basic idea of the mechanism for shuttle transport is that the electrostatic energy, due to the tunneling of electrons from the leads to the mobile metallic nanoparticle, can be large enough to deform the system. When the leads are voltage biased,

above the critical voltage V_C, the charged nanoparticle is pushed by the bias voltage towards the opposite electrode where reverse charging takes place, and consequently the nanoparticle experiences reverse motion. In this sense the metallic nanostructure acts as a shuttle of electrons. In the proposal of Gorelik and co-workers oscillations of the shuttle are driven via self-excitations, originating from the work done which is determined by correlations between the charge of the nanoparticle and its position. The shuttle nanostructure is *assymmetric* in the sense that a bias voltage is needed to drive the system, thus the electrical field serves as a breaking symmetry agent.

In the shuttle mechanism of charge transport, Coulomb blockade phenomena play an important role as they limit the number of electrons inside the nanoparticle due to the high energy required to add an electron. For systems with continuous energy spectra, the charging energy is $E_c = Q^2/2C$, where Q is the extra charge and C the capacitance of the island [56]. The main feature of the shuttle phenomenon is that a constant potential difference, applied between two fixed electrodes, leads to a dynamical instability that causes the metal nanoparticle to oscillate. In the limit of low dissipation, a dc current through the system, induced by the voltage drop between the electrodes, becomes proportional to the frequency of the mechanical oscillations [49],

$$I = 2eNf \qquad \text{where} \qquad N = \left[\frac{CV}{e} + \frac{1}{2}\right], \tag{1.28}$$

e is the elementary charge, V is the voltage and f is the frequency of the nanoparticle.

The sequential transfer of electrons in shuttling phenomena was described in the framework of classical mechanics and stochastic processes, in this case the electron dephasing time τ_0 is much shorter than the tunneling charge relaxation time $R_T C$, where R_T is the tunneling resistance of the double junction [56]. The idea of shuttle phenomena was also extended to the quantum realm [57–60].

Nanoelectromechanical shuttle systems have been also studied in the regime of ac excitation and several interesting effects on the transport properties and the dynamics of the shuttle system have been found [61–65]. In particular, a shuttle structure driven by a time-dependent bias voltage has been considered in Refs. [66, 67]. It was shown that in case of *assymetric configuration* such a setup can act as a rectifier, where the intensity of the dc current depends on the ratio between the frequency of the external oscillating voltage and the eigenfrequency of the mechanical subsystem. In Paper IV we investigate the dynamics of a spatially symmetric shuttle-system subjected to an ac gate voltage. We demonstrate that, despite the lack of a bias voltage, a shuttle dc current can be generated. This mechanism of electron transport is an extension of the shuttle transport proposed by Gorelik *et al.* [49] in which the direction of the shuttle transport does not rely on the presence of any bias voltage.

1.4.6 Parametric resonance

In Paper IV we introduce a new form of shuttle transport of electrons. In this novel idea, the phenomenon of parametric resonance is a crucial point. In this section we discuss in some detail the main features of parametric resonance.

According to the conventional classification of oscillations by their method of excitation, oscillations are denominated forced when the dynamical system is subjected

to an external periodic input. If the frequency of the external force ω is close to the frequency oscillator ω_0, the amplitude of the steady-state forced oscillations can reach a large value. This phenomenon is called *resonance* [68].

Another way to excite oscillations in a system consists of a periodic variation of some parameters of the system; oscillations are called parametric when the amplitude of oscillation caused by the periodic modulation of some parameters, to which the motion of the system is sensitive, increases steadily.

To discuss the parametric resonance quantitatively we consider an undamped free oscillator in which the spring constant experiences a periodic modulation, *i.e.*, the frequency of the oscillator is time-dependent, $\omega(t)$, and differs slightly from the natural frequency of the resonator ω_0. It can be described as

$$\omega^2(t) = \omega^2(1 + h\cos(\Omega t)), \tag{1.29}$$

where the constant $h \ll 1$ is referred to as the parametric modulation amplitude and Ω is the modulation frequency. Parametric resonance is strongest when the modulation frequency of $\omega(t)$ is nearly twice ω_0. Therefore we set $\Omega = 2\omega_0 + \epsilon$, where $\epsilon \ll \omega_0$.

The solution of the equation motion for the free oscillator,

$$\ddot{x} + \omega^2[1 + h\cos(2\omega_0 + \epsilon)t]x = 0, \tag{1.30}$$

can be cast in the form

$$x = a(t)\cos((\omega_0 + \epsilon/2)t) + b(t)\sin((\omega_0 + \epsilon/2)t), \tag{1.31}$$

where the functions $a(t)$ and b(t) are time-dependent functions which vary slowly in comparison with the trigonometrical factors.

After substitution of Eq. (1.31) into Eq. (1.30), a perturbative analysis indicates that the instability frequency window in which the parametric resonance occurs is (see details in Ref. [69])

$$-h\omega_0/2 < \epsilon < h\omega_0/2 \tag{1.32}$$

At the parametric resonance the equilibrium becomes unstable and the system is excited[2], in this regime the amplitude of oscillations increases. The growth of both amplitude and energy of oscillations during parametric excitation is provided by the work of forces that periodically change the parameter. The energy transfer process to the dynamical system during parametric excitation can also take place when the frequency of the periodic modulated parameter fulfill the following condition,

$$\omega = 2\omega_0/n, \tag{1.33}$$

where $n = 1, 2, ...$ In general, the amount of energy given to the oscillating system decreases with the order n of the parametric resonance.

An important difference between parametric and forced oscillations is the way in which the growth of energy depends on the energy already stored in the system. In the regime of parametric excitation the increment of energy is proportional to the square of the amplitude, *i.e.*, to the energy stored in the system. In case of forced

[2]Any small disturbance from equilibrium leads to a parametric instability

oscillations, the increment of energy is proportional to the amplitude of oscillations, *i.e.*, to the square root of the energy.

Energy losses due to dissipative forces are also proportional to the energy stored in the system. Therefore, in the regime of parametric oscillations the increment of energy caused by a periodic variation of some parameters and the dissipative losses are proportional to the square of the amplitude, thus their ratio is independent of the amplitude of oscillation. As a consequence, parametric resonance takes place when the increment of energy exceeds the amount of energy dissipated. Once the this threshold value has been overcome, the frictional losses of energy cannot affect the growth of the amplitude. In linear systems, the amplitude of the parametrically excited oscillations grows without any limit. However, in real systems, the growth amplitude is restricted by nonlinearities. For a review about parametric resonance, the reader is referred to Refs. [68, 69].

1.5 Thesis overview

The scientific results presented in this thesis are based on Papers I-IV. This thesis is organized in the following manner. In Chapter 2, we summarize the material presented in Papers I-II where we study a mechanism to cool the quantized vibrations of a suspended nanowire in a voltage-biased superconducting junction. We focus our attention in the electromechanical coupling generated by a homogeneous magnetic field. In Chapter 3, we consider the same voltage-biased nanoelectromechanical systems as in Chapter 2, but now extend the analysis to a case in which the nanoelectromechanical Josephson junction is subjected to a nonuniform magnetic field. In Chapter 4, we study parametric excitation of a dc current in a symmetric shuttle-system. Finally, in Chapter 5, we provide the summary of the thesis.

CHAPTER 2

Cooling of a suspended nanowire

It is the objective of this Chapter to discuss the conditions necessary for ground state cooling of an oscillating nanowire suspended between two voltage-biased superconducting leads. In our description we consider the high transparency limit of the nanoelectromechanical Josephson junction and use the language of quantum mechanics in order to treat the oscillating nanowire. Below we describe the proposed cooling scheme presented in Papers I-II, where the possibility to cool the vibrations of the nanoresonator relies on the transfer of energy from the mechanical vibrations of the nanowire to the electronic quasiparticle bath in the superconducting leads. This energy transfer process is achieved by inducing transitions between the bound Andreev levels. In Papers I-II we analyze the situation in which these transitions can be accomplished by applying a uniform magnetic field perpendicular to the long axis of the nanobeam.

2.1 System and electromechanical coupling

The diagram in Fig. 2.1 is a schematic illustration of a superconducting hybrid nanodevice, a superconductor-normal-superconductor (S-N-S) *nanoelectromechanical Josephson junction* driven by a dc voltage bias V in an homogeneous magnetic field. The junction consists of a metallic carbon nanotube suspended between two voltage-biased superconducting leads. In such a geometry, the nanotube is simultaneously serving as a mechanical resonator and as a weak link between the superconducting electrodes. This double functionality of the metallic nanotube can be explained as follows:

- By considering the system as a doubly-clamped beam, the nanowire forms a mechanically compliant element.
- By considering the system as an electronic device, the metallic nanowire acts as a weak link between two superconductors.

It is worth mentioning that without any external influence (*e.g.* electromagnetic radiation, magnetic field, electric field, electrostatic gates, *etc.*) there is no electromechanical coupling between the mechanical and electronic subsystems and they remain independent each other. The properties of each subsystem has already been discussed (see Chapter 1). However, by applying a uniform magnetic field perpendicular to the

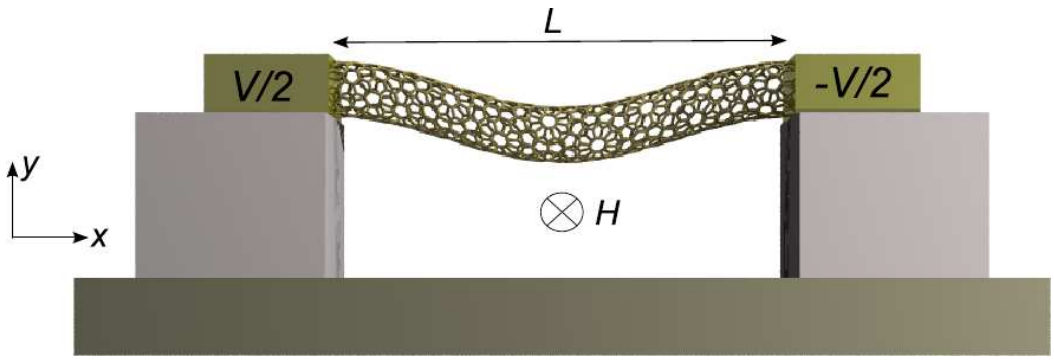

Figure 2.1: S-N-S nanoelectromechanical Josephson junction in a magnetic field.

direction of the current carried by the Andreev states, the Lorentz force couples vibrations in the carbon nanotube to the current flowing through it, *i.e.*, the mechanical and electronic subsystems are interconnected. This electromechanical coupling opens an energy transfer channel through which vibrational energy from the harmonic oscillator can be transferred into the electronic Andreev levels. The corresponding energy uptake of the electronic subsystem is later released into the continuum states, leading to an effective cooling of the resonator.

In order to describe in more detail the energy transfer mechanism, the dynamics of the voltage-biased Andreev levels coupled to the mechanical subsystem is presented in Fig. 2.2. This plot is a schematic diagram of the evolution of the coupled electromechanical system. Here, the applied dc voltage bias V causes the superconducting phase difference to evolve in time in accordance with equation (1.24), and drives the adiabatic motion of the Andreev levels according to Eqs. (1.26) and (1.27). In Fig. 2.2, the evolution in time of the Andreev levels is indicated by solid lines and correspond to the periodic trajectories definied by $E_{\pm}(\phi(t)) = \pm\sqrt{1 - D\sin^2(\phi(t)/2)}$, the period of the energy spectrum is $T_V = \pi\hbar/(eV)$. In our analysis, we assume that the thermal energy is much smaller than the initial separation between the levels, $k_B T \ll 2\Delta_0$. This assumption implies that at the start of the period ($t = 0$) the lower Andreev level (•) is populated while the upper one is empty (◦). In Papers I-II we analyze the case in which a transverse magnetic field couples the vibrations of the nanowire to the Andreev levels, and transitions from the lower to the upper Andreev level might occur by absorption of a quantum of mechanical energy $\hbar\omega$. The probabilily of absorption of a quantum of mechanical energy is increased at time $t \approx t_0$ when the electromechanical coupling in the system is maximum and the energy gap between the Andreev levels attains its minimum value

$$E_{gap} = 2\Delta_0\sqrt{R}\,. \tag{2.1}$$

On condition that the quantum of mechanical energy of the nanoresonator,

$$E_{mech} = \hbar\omega \tag{2.2}$$

matches the minimum gap value between Andreev levels,

$$2\Delta_0\sqrt{R} = \hbar\omega\,. \tag{2.3}$$

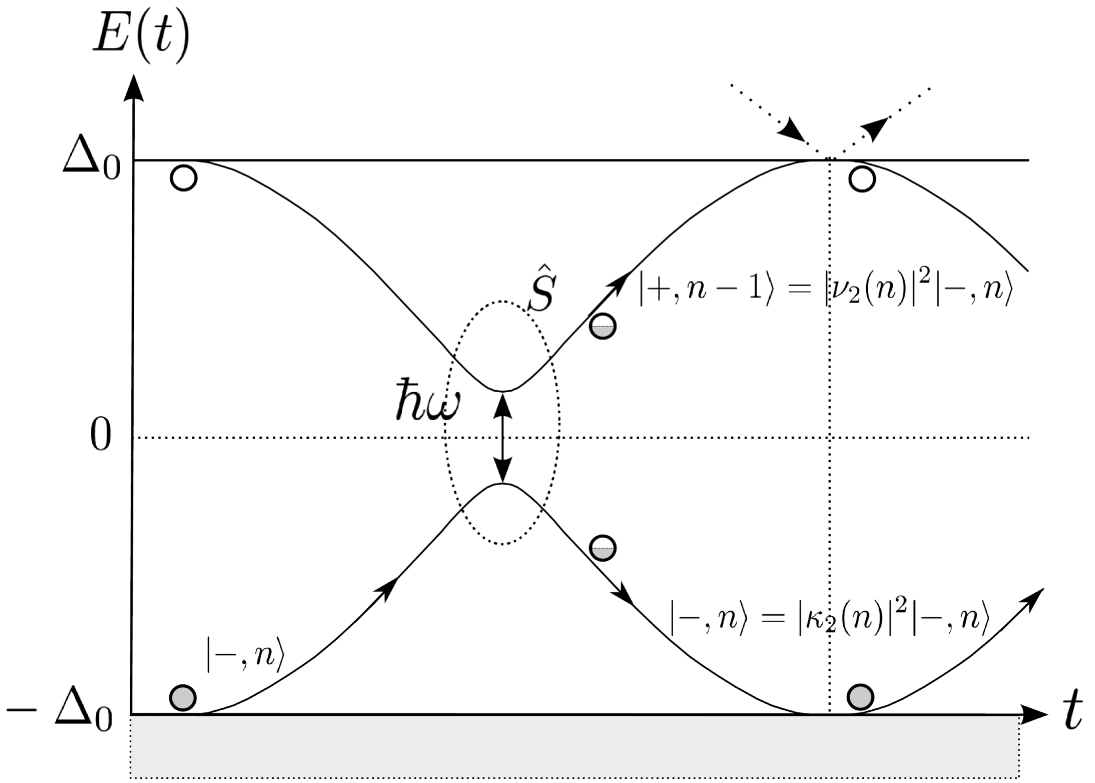

Figure 2.2: Dynamics of the Andreev levels coupled to the mechanical subsystem. Here, $|\pm, n\rangle = |\pm\rangle \otimes |n\rangle$ denote the states of the junction; $|\pm\rangle$ labels the upper and lower Andreev level, and $|n\rangle$ is the quantum state of the oscillator. At the start of the period, a pair of Andreev states are created and their occupation depends on the distribution of quasiparticle excitations in the leads. As $k_B T \ll 2\Delta_0$, the upper Andreev level is empty ($\circ$) while the lower one is the populated ($\bullet$). These bound states carry current through the nanodevice. Under conditions of adiabatic motion $eV \leqslant 4R\Delta_0$, they evolve in time with period T_V. Transitions from $|-, n\rangle$ to $|+, n-1\rangle$ occur when the energy gap between the levels matches the mechanical energy quantum $\hbar\omega$ and, they are described through the scattering matrix $\hat{S}$. After one period, the Andreev states merge with the comtinuum states (arrows) and new states, orthogonal to the old states are created. Here, the electronic subsystem is reset at the start of each period. See discussion in the text.

Then, transitions from the lower branch to the upper branch can occur and the levels would become mixed. Afterwards, at the end of one period, $t \approx t_V$, the bound Andreev levels merge with the continuum states in the superconducting leads and new states are formed. Here we assume that the Andreev levels are reset at the start of each period (see discussion in Section 2.11) and the energy transfer process is repeated again over many periods leading to an effective cooling of the nanowire. Note that the mechanical subsystem is not affected by the dissolution of the Andreev levels into the continuum spectrum in the leads, thus, they can be overcooled in the subsequent periods.

Finally, in order to complete our cooling scheme, a few words about adiabatic motion of the Andreev levels under weak bias must be mentioned. As discussed earlier (see Section 1.4.3), the voltage-biased Andreev levels will move adiabatically within the superconductor energy gap on condition that $2eV \ll \Delta_0$ (*cf.* Eq. (1.26)). In addition, our proposal for cooling implies that without any electromechanical coupling, the population of the Andreev levels will remain constant at any time. As a consequence, the applied voltage should be restricted so that it can not induce Landau-Zener transitions at time $t \approx t_0$. It turns out that the applied bias must be less than or equal to a certain critical voltage in order to fulfill the conditions for adiabatic motion and steady population of the Andreev levels without any electromechanical coupling. It can be estimated (as discussed further in Appendix 1) as

$$V \leqq V_C = 4\Delta_0 R/e\,. \tag{2.4}$$

In Papers I-II it is shown that through the energy mechanism described above the nanowire may be cooled to its ground state. In the following sections we give a more in depth description of the applied model and mathematical methods used in our research.

2.2 Mechanical Hamiltonian

In our analysis, the vibrating nanowire is modeled as a quantum harmonic oscillator, taking only the fundamental bending mode into account. In the framework of quantum mechanics, the Hamiltonian for the harmonic oscillator is [70]

$$\hat{H}_{mech} = \hbar\omega \hat{b}^\dagger \hat{b}\,. \tag{2.5}$$

Here, $\hbar$ is the Planck constant and ω is the fundamental frequency. The operator $\hat{b}^\dagger(\hat{b})$ creates (annihilates) one quantum of vibrational energy $\hbar\omega$ of vibronic energy. These operators satisfy the commutation relation $[\hat{b}, \hat{b}^\dagger] = 1$.

2.3 Electronic Hamiltonian

As discussed earlier, from the electronic point of view, the nanowire constitutes a weak link for a short S-N-S Josephson junction. This type of junctions can experience Andreev reflections at the metal and superconductors interfaces. Therefore, the electronic degrees of freedom can be cast in the form of a pair of bound Andreev states.

The spatial extent of these states will be of the order of the superconducting coherence length ξ. In our analysis we assume that the coherence length is much larger than the length of the nanowire L. Assuming that the adiabatic conditions are fulfilled Eqs. (1.26) and (2.4), the Andreev levels describe a two-level system and the electronic Hamiltonian can be written in terms of temporally evolving energy levels. This two-level Hamiltonian reads

$$\hat{H}_{ele}(t) = \pm\mathcal{E}(\phi(t))\hat{\sigma}_z + \Delta_0\sqrt{R}\sin(\phi(t)/2)\hat{\sigma}_x\,. \tag{2.6}$$

Here, the first term $\mathcal{E}(\phi(t)) = \Delta_0\cos(\phi(t)/2)$ is the Andreev level for a single state in a transparent junction. The second term is the energy contribution of an impurity in the carbon nanotube with reflection coefficient R and $\hat{\sigma}_i$ ($i = x, y, z$) are the Pauli matrices. The physical interpretation of these two terms is the following: For the completely transparent junction, the upper level of backward travelling electrons and the lower level of forward moving electrons are independent of each other when there is no normal scattering. As soon as the impurity is present, it reflects electrons and the Andreev levels become coupled, therefore the energy degeneracy at $\phi(t) = \pi$ is lifted and an energy gap of size $E_{gap} = 2\Delta_0\sqrt{R}$ appears in the quasiparticle energy spectrum. This qualitative description is in agreement with solution of the Bogoliubov-de Gennes equations given by Eq. (1.20).

2.4 Interaction Hamiltonian

In our proposal the externally applied magnetic field is used for coupling the Andreev levels to deflections of the nanowwire. In this case, the Lorentz force that couples the mechanical and electronic degrees of freedom in the system is given by

$$F = HIL, \tag{2.7}$$

where H is the applied magnetic field, I the current across the junction and L the length of the suspended part of the mechanical nanoresonator. Consequently, the time-dependent interaction term reads

$$\hat{H}_{int}(t) = H\hat{I}(\phi(t))L\hat{y}\,, \tag{2.8}$$

where $\hat{y}$ is the resonator position operator and $\hat{I}(\phi(t))$ the phase-dependent current operator given by Eq. (1.22). The displacement of the nanoresonator in terms of the creation and annihilation operators is

$$\hat{y} = y_0[\hat{b}^\dagger + \hat{b}]\,. \tag{2.9}$$

In Eq. (2.9), y_0 is the amplitude of the zero-point oscillations in the nanoresonator and it is defined as

$$y_0 = \sqrt{\hbar/(2m\omega)}\,. \tag{2.10}$$

By substituting Eq. (2.9) and Eq. (1.22) into Eq. (2.8), the interaction Hamiltonian becomes

$$\begin{aligned}\hat{H}_{int}(t) &= H\frac{2e}{\hbar}\frac{\partial\mathcal{E}(\phi(t))}{\partial\phi(t)}Ly_0[\hat{b}^\dagger + \hat{b}]\hat{\sigma}_z \\ &= \frac{e\Delta_0}{\hbar}LHy_0\sin(\phi(t)/2)[\hat{b}^\dagger + \hat{b}]\hat{\sigma}_z\,.\end{aligned} \tag{2.11}$$

In order to simplify the notation in Eq. (2.11), a dimensionless magnetic flux can be introduced

$$\Phi = 2LH\pi y_0/\Phi_0\,. \tag{2.12}$$

Where

$$\Phi_0 = h/2e\,, \tag{2.13}$$

is the magnetic flux quantum. After the introduction of these quantities, the interaction Hamiltonian in Eq. (2.11) reads

$$\hat{H}_{int}(t) = \underbrace{\Delta_0\Phi\sin(\phi(t)/2)}_{g(\phi(t))}[\hat{b}^\dagger + \hat{b}]\hat{\sigma}_z\,. \tag{2.14}$$

From the last equation, it is concluded that the coupling term $g(\phi(t))$ attains its maximum at $\phi(t) = \pi$, which coincides with a minimal energy gap between Andreev levels. Since the energy scales of the superconductive order parameter and the mechanical vibrations are very different, $2\Delta_0 \gg \hbar\omega$, transitions between the Andreev levels are most probable when the electromechanical coupling is strongest and the energy gap between the Andreev levels equals the energy scale set by the harmonic oscillator, *i.e.*, when the resonance condition[1],

$$\hbar\omega = 2\Delta_0\sqrt{R}\,, \tag{2.15}$$

is satisfied. Consequently, transitions between Andreev levels are likely to occur when $\phi(t) = \pi$ (at $t = t_0$) as it can be seen in Fig. **??**.

2.5 Total system Hamiltonian

The Hamiltonian describing the system is

$$\begin{aligned}\hat{H}_{sys}(t) &= \hat{H}_{mech} + \hat{H}_{ele}(t) + \hat{H}_{int}(t)\,,\\ &= \hbar\omega\hat{b}^\dagger\hat{b} + \mathcal{E}(\phi(t))\hat{\sigma}_z + \Delta_0\sqrt{R}\sin(\phi(t)/2)\hat{\sigma}_x + \Delta_0\Phi\sin(\phi(t)/2)[\hat{b}^\dagger + \hat{b}]\hat{\sigma}_z\,.\end{aligned}$$

To proceed further, the system Hamiltonian given in Eq. (2.16) is expressed in the basis where the energy of the two electronic states takes the form

$$E(t) = \pm\Delta_0\sqrt{1 - D\sin^2(\phi(t)/2)}\,, \tag{2.16}$$

and the space is spanned by the states $\Psi_\pm(\phi(t))$. In this space the Hamiltonian of the system reads,

$$\hat{H}_{eff}(t) = \hbar\omega\hat{b}^\dagger\hat{b} + \Delta_0\sqrt{1 - D\sin^2(\phi(t)/2)}\hat{\tau}_z + \Delta_0\Phi\sin(\phi(t)/2)[\hat{b}^\dagger + \hat{b}]\hat{\tau}_x\,. \tag{2.17}$$

In the last equation τ_i ($i = x, y, z$) are the Pauli matrices in the space of the wave functions $\Psi_\pm(\phi(t))$. At the resonant phase $\phi(t) = \pi$, the Andreev states $\psi_\pm(\phi(t) = \pi)$ with energies $E_\pm(\phi(t) = \pi) = \pm\Delta_0\sqrt{R}$ are superpositions of symmetric and antisymmetric states carrying current in opposite directions.

[1]This condition requires the weak link to have a high transparency coefficient D [71].

2.6 Transition between Andreev levels

The description of the process continues by estimating the transition probabilities between Andreev levels through the absorption of one quantum of mechanical energy over one period. In order to calculate them, the rotating wave approximation (RWA) is applied to Eq. (2.17) (see discussion in Appendix 2). In the RWA framework the Hamiltonian becomes

$$\hat{\mathcal{H}}_{eff}(t) = \begin{pmatrix} E(t) - \hbar\omega/2 & \Delta_0\Phi\sin(\phi(t)/2)\hat{b} \\ \Delta_0\Phi\sin(\phi(t)/2)\hat{b}^\dagger & -E(t) + \hbar\omega/2 \end{pmatrix} . \tag{2.18}$$

By using the Josephson relation, Eq. (1.24), it may be concluded that the transitions between Andreev levels are more likely to occur at $t_0 = \pi\hbar/2eV$ ($\phi(t_0 = \pi)$) when the electromechanical coupling (off-diagonal elements of the matrix) is maximum. Therefore, the analysis of Eq.(2.18) can be restricted to the vicinity of this time. By performing a series analysis, the second order Taylor expansion of the energy $E(t)$ around t_0, where $|E(t_0)| = \hbar\omega/2$ and $\dot{E}(t_0) = 0$, generates the following dimensionless differential equation

$$i\partial_\tau \begin{pmatrix} c_{+,n-1}(\tau) \\ c_{-,n}(\tau) \end{pmatrix} = \begin{pmatrix} \tau^2 & \Gamma\sqrt{n} \\ \Gamma\sqrt{n} & -\tau^2 \end{pmatrix} \begin{pmatrix} c_{+,n-1}(\tau) \\ c_{-,n}(\tau) \end{pmatrix} , \tag{2.19}$$

for the probability amplitudes $c_{\pm,n}(\tau)$ of finding the state of the system in the upper(+)/lower(-) Andreev level with the oscillator in the state n. The dimensionless variables introduced in Eq. (2.19) are

$$\tau = (t - t_0)(\xi/\hbar)^{1/3} , \tag{2.20}$$

$$\Gamma = \frac{\Phi\Delta_0}{\hbar\omega}\left(\frac{V_c}{V}\right)^{2/3} , \tag{2.21}$$

$$\xi = \left.\frac{\partial^2 E(t)}{\partial t^2}\right|_{t_0} = \frac{D(\hbar\omega)^3}{\hbar^2}\left(\frac{V}{V_c}\right)^2 . \tag{2.22}$$

The coupling terms responsible for the interlevel transitions correspond to the off-diagonal elements in Eq. (2.19). They are proportional to Γ and can be estimated by considering the following parameters:

1. Quantum of mechanical energy $\hbar\omega$ =1 μ eV
2. Superconducting gap $\Delta_0 = 10\hbar\omega$ =10 μ eV
3. Amplitude of the zero-point oscillations y_0 =20 pm
4. Length of the metallic nanotube L =100 nm
5. Applied magnetic field[2] H =1 T
6. Critical voltage V_c =10^{-7} V

[2]Such a magnetic field is not going to destroy the superconducting properties of thin film leads. In these materials the critical magnetic field H_c can be greater than 1 T [72].

By substituting these parameters into Eq. (2.21) and taking into account that in the adiabatic regime $V \lesssim V_c$, the numerical analysis yields $\Gamma \ll 1$. As a consequence, by focusing on the infinitesimal interval $(-\delta\tau, \delta\tau)$ around the transition point $\tau_0 = 0$, the parameter Γ may be considered as a perturbation of $|c_{-,n}(-\delta\tau)|^2 = 1$ and the probability to find the system in the upper Andreev level at $\delta\tau$ after the resonant point is,

$$|c_{+,n-1}(\delta\tau)|^2 \approx \pi\Gamma^2 n\,. \tag{2.23}$$

Therefore, the probability of a transition between the Andreev levels is linear with the initial vibronic population of the mechanical resonator after crossing the resonance. From Eq. (2.20) and Eq. (2.22), the characteristic time scale of the electromechanical interactions can be estimated as

$$\delta t \approx (\hbar\omega\Phi/\Delta_0)^{1/2}\hbar/(eV) \ll 20\,\mathrm{ns}\,. \tag{2.24}$$

The efficiency of the energy transfer process (cooling mechanism) depends on the competition between the probability of transitions between the Andreev levels and the thermal damping. This analysis will be done by studying the density matrix of the system.

2.7 Density Matrix Analysis

In this section, the dynamics of the coupled electromechanical system is described in the framework of the density matrix formalism. Here we investigate the form in which the nanoresonator is affected by interactions with the external heat bath. In our description, the interaction of the mechanical subsystem with the thermal environment is modeled through the following integral collision,

$$\hat{\mathfrak{L}}(\hat{\rho}) = -(1+n_B)\left(\hat{b}^\dagger\hat{b}\hat{\rho} + \hat{\rho}\hat{b}^\dagger\hat{b} - 2\hat{b}\hat{\rho}\hat{b}^\dagger\right) - n_B\left(\hat{b}\hat{b}^\dagger\hat{\rho} + \hat{\rho}\hat{b}\hat{b}^\dagger - 2\hat{b}^\dagger\hat{\rho}\hat{b}\right)\,, \tag{2.25}$$

where $n_B = (\exp[\hbar\omega/k_BT]-1)^{-1}$ is the corresponding occupation number of the oscillator at temperature T. The evolution of the density matrix over one period depends on which regime is studied:

1. In the adiabatic regime, where the Andreev levels evolve independently and the system only interacts with the environment, the evolution of the density matrix is determined by

$$\frac{\partial\hat{\rho}(t)}{\partial t} = -\frac{i}{\hbar}\left[\hat{H}_{eff}(t), \hat{\rho}(t)\right] + \frac{\gamma}{2}\hat{\mathfrak{L}}(\hat{\rho}(t))\,, \tag{2.26}$$

   where $\gamma = \omega/Q$ is the thermal damping rate of the vibrational modes and Q denoting the quality factor.

2. In the transition regime, where the levels interact for a short interval of time $(-\delta t, \delta t)$, the dynamics of the density matrix is described through the expression

$$\hat{\rho}(t_0+\delta t) = \hat{S}\hat{\rho}(t_0-\delta t)\hat{S}^\dagger\,. \tag{2.27}$$

Here, the unitary scattering matrix $\hat{S}$ is introduced and it has the following structure

$$\hat{S} = \begin{pmatrix} \kappa_1(\hat{n}) & i\frac{\nu_1(\hat{n})}{\sqrt{\hat{n}+1}}\hat{b} \\ i\hat{b}^\dagger\frac{\nu_2(\hat{n}+1)}{\sqrt{\hat{n}+1}} & \kappa_2(\hat{n}) \end{pmatrix} . \tag{2.28}$$

In the scattering $\hat{S}$-matrix the term

$$\hat{n} = \hat{b}^\dagger\hat{b} , \tag{2.29}$$

corresponds to the number operator of mechanical vibrons. The subscripts $1, 2$ refer to the upper(+)/lower(-) Andreev level respectively. The elements of the S-matrix are:

- $\kappa_{i=1,2}(\hat{n})$ is the probability amplitude for the electronic subsystem to remain in the top/bottom electronic branch.
- $\nu_{i=1}(\hat{n})$ is the probability amplitude for the electronic subsystem to be found in lower level after the interaction.
- $\nu_{i=2}(\hat{n})$ is the probability amplitude for the electronic subsystem to be found in upper level after crossing the resonant point.

These coefficients satisfy the relationship

$$|\kappa_{i=1,2}(n)|^2 + |\nu_{i=1,2}(n)|^2 = 1 . \tag{2.30}$$

From this analysis it is possible to conclude that

$$|c_{+,n-1}(\delta\tau)|^2 = |\nu_2(n)|^2 \simeq \pi n\Gamma^2 . \tag{2.31}$$

Additionally, $|\nu_2(n)|^2 = |\nu_1(n-1)|^2$ which follows from the symmetry of Eq. (2.19). As outlined before the probability of Andreev level transitions is proportional to the magnetic field and the quantum state of the oscillator.

2.8 Evolution of the density matrix

In order to evaluate the evolution of the density matrix during a single period, it is assumed that the thermal energy is much smaller than the initial gap between the Andreev levels, $k_BT \ll 2\Delta_0$, and the following boundary conditions:

$$\hat{\rho}(t = nT_V + \varepsilon) = \begin{pmatrix} 0 & 0 \\ 0 & 1 \end{pmatrix} \otimes \hat{\rho}_p(nT_V) . \tag{2.32}$$

$$\hat{\rho}_p(nT_V) = \mathrm{Tr}_{el}\hat{\rho}(nT_V - \varepsilon) . \tag{2.33}$$

Here

$$T_V = \pi\hbar/eV . \tag{2.34}$$

In the previous expressions $n = 0, 1, 2, \cdots$, is an integer which labels the number of periods and ε is infinitesimal time around nT. With these considerations at the start of the period, the initial density matrix

$$\hat{\rho}^{in} \equiv \hat{\rho}(t = nT_V + \varepsilon) , \tag{2.35}$$

will evolve during one period into

$$\hat{\rho}^f \equiv \hat{\rho}(t = [n+1]T_V - \varepsilon)\,. \tag{2.36}$$

In the limit of high mechanical quality factor ($Q \sim 10^5$ [73]) the mechanical subsystem is weakly coupled to the external thermal environment and the interaction between both systems can be treated as a perturbative term in Eq. (2.26). From standard perturbation theory, the time evolution of the density matrix over one period is

$$\hat{\rho}^f = \hat{S}\hat{\rho}^{in}\hat{S}^\dagger + \frac{\gamma}{2}\frac{T_V}{2}\hat{S}\hat{\mathfrak{L}}(\hat{\rho}^{in})\hat{S}^\dagger + \frac{\gamma}{2}\frac{T_V}{2}\hat{\mathfrak{L}}(\hat{S}\hat{\rho}^{in}\hat{S}^\dagger)\,. \tag{2.37}$$

Now, in light of the above boundary conditions (Eq. (2.32) and Eq. (2.33)), the expression for the evolution of the density matrix after one period at time $t = [n+1]T_V + \varepsilon$ is

$$\hat{\rho} = \begin{pmatrix} 0 & 0 \\ 0 & 1 \end{pmatrix} \mathrm{Tr}_{el}\left(\hat{S}\hat{\rho}^{in}\hat{S}^\dagger + \frac{\gamma}{2}\frac{T_V}{2}\hat{S}\hat{\mathfrak{L}}(\hat{\rho}^{in})\hat{S}^\dagger + \frac{\gamma}{2}\frac{T_V}{2}\hat{\mathfrak{L}}(\hat{S}\hat{\rho}^{in}\hat{S}^\dagger)\right). \tag{2.38}$$

The stationary regime is achieved when

$$\hat{\rho}(nT_V + \varepsilon) = \hat{\rho}([n+1]T_V + \varepsilon). \tag{2.39}$$

It turns out that the stationary density matrix at time $t = nT_V + \varepsilon$ has the form

$$\hat{\rho}^{st} = \sum_{n=0}^{\infty} P_n^{st} \begin{pmatrix} 0 & 0 \\ 0 & 1 \end{pmatrix} |n\rangle\langle n|\,. \tag{2.40}$$

Hence, in the stationary regime

$$\sum_{n=0}^{\infty} P_n^{st} \begin{pmatrix} 0 & 0 \\ 0 & 1 \end{pmatrix} |n\rangle\langle n| = \begin{pmatrix} 0 & 0 \\ 0 & 1 \end{pmatrix} \mathrm{Tr}_{el}\left(\hat{S}\hat{\rho}^{st}\hat{S}^\dagger + \frac{\gamma}{2}\frac{T_V}{2}\hat{S}\hat{\mathfrak{L}}(\hat{\rho}^{st})\hat{S}^\dagger + \frac{\gamma}{2}\frac{T_V}{2}\hat{\mathfrak{L}}(\hat{S}\hat{\rho}^{st}\hat{S}^\dagger)\right). \tag{2.41}$$

In the last equations, P_n^{st}, is the stationary distribution of mechanical excitations.

2.9 Results

In order to find the stationary probability distribution of mechanical excitations a numerical analysis of Eq. (2.41) must be done. This can be achieved by projecting Eq. (2.38) on the mechanical space and expressing the result in matrix form. Through this procedure, a matrix equation for the probability distribution of vibronic states is obtained,

$$\mathbf{A}\mathbf{P_n} = \boldsymbol{\zeta}\mathbf{P_n}. \tag{2.42}$$

Here, $\mathbf{P}$ is the probability distribution of vibronic modes in the nanowire, $\mathbf{A}$ is the probability matrix generated from Eq. (2.38) and $\boldsymbol{\zeta}$ is an eigenvalue. Hence, finding the stationary vibronic distribution, P_n^{st}, is an eigenvalue problem.

We can evaluate the average population of vibrational modes $\langle n\rangle$ when the population of the vibrational modes does not change over one period, *i.e.*, in the stationary

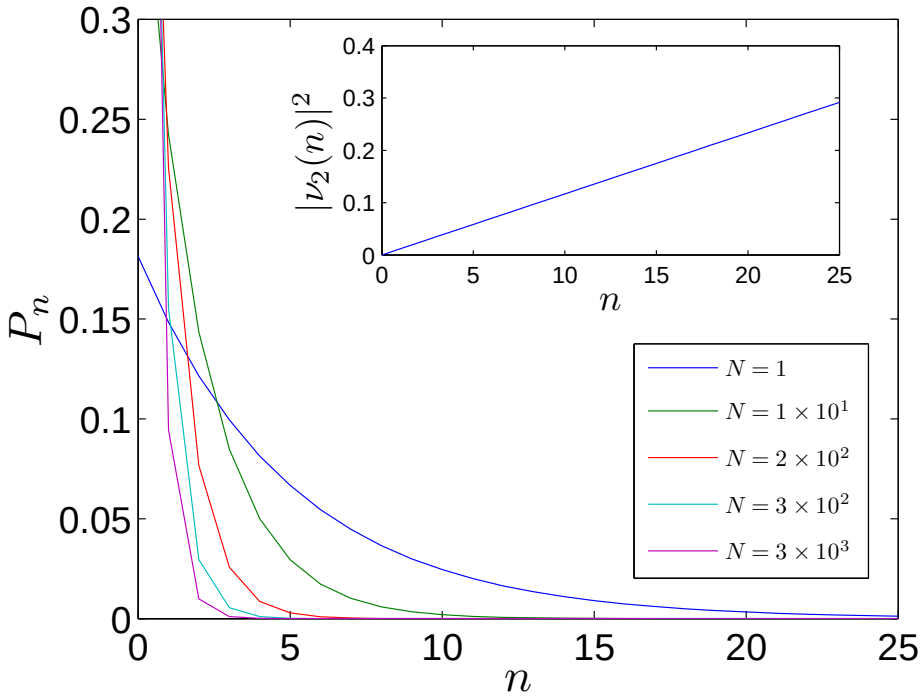

Figure 2.3: Probability distribution of the population of the vibrational modes P_n in the system. In the plot, N labels the number of periods and the inset displays the transition probability as a function of the occupation number of the quantum state of the oscillator n. The curve $N = 1$ (blue) corresponds to the initial thermal distribution, $P_n^{thermal} \propto e^{-\hbar\omega n/k_B T}$. The oscillating carbon nanotube is cooled to its motional ground state $\langle n \rangle \lesssim 1$ after 3000 periods (curve in magenta). The system parameters are: $k_B T = 5\hbar\omega$, V_c =10^{-7} V, $\hbar\omega$ =10^{-6} eV, $\Delta_0 = 10\hbar\omega$, y_0 =20 pm, L =100 nm, H =1 T, $Q = 10^5$ and $T_V = \pi\hbar/eV \sim$20 ns.

regime. From the mathematical point of view, it corresponds to finding the probability distribution with eigevalue $\zeta = 1$. By calculating the expectation value of the vibronic occupation number,

$$\langle n \rangle = \sum_n P_n n \,. \tag{2.43}$$

The corresponding evolution of the distribution of the vibrational modes is shown in Fig. 2.3. As can be seen clearly, the energy transfer process discussed above has lowered the vibronic excitations from the originally thermal distributed (blue) to the stationary one (magenta). The metallic carbon nanotube is effectively cooled as

$$\langle n_{thermal} \rangle \sim 4.5 \gg \langle n_{st} \rangle \sim 0.1 \,. \tag{2.44}$$

This result is confirmed by the perturbative solution,

$$\langle n_{st} \rangle \simeq \frac{n_B}{Q\Phi^2} \frac{\hbar\omega}{\Delta_0} \left(\frac{V}{V_c} \right)^{1/3} \sim 0.1 \,. \tag{2.45}$$

The stationary distribution in Fig. 2.3 corresponds to $T_{eff} < T$, where T_{eff} is the *effective* temperature of the metallic carbon nanotube in the stationary regime.

2.10 DC current through the junction

In Paper II the possibility to probe the stationary distribution of the mechanical subsystem is considered. There we suggest studying the dc current through the nanomechanical weak link as this directly measures the population of the vibrational modes. To show this we evaluate the dc current (on resonance) induced by the transition between Andreev levels over one period when the mechanical subsystem has reached the stationary regime. This current arises due to the scattering process which promotes transition from the lower to the upper Andreev level. This process will result in a net charge transfer through the nanostructure. We can evaluate the total current (over a period) as

$$I_{dc} = \frac{2e}{\hbar} \frac{2}{T_V} \Bigg[\int_0^{T_V/2} \frac{\partial E_-(\phi(t))}{\partial \phi(t)} \mathrm{d}t + (1 - P_{stat}) \int_{T_V/2}^{T_V} \frac{\partial E_-(\phi(t))}{\partial \phi(t)} \mathrm{d}t + \\ + P_{stat} \int_{T_V/2}^{T_V} \frac{\partial E_+(\phi(t))}{\partial \phi(t)} \mathrm{d}t \Bigg] \,, \tag{2.46}$$

where, P_{stat} is the total probability for the system to be scattered from the lower energy level to the upper one. Since n quanta of mechanical energy are excited with probability $P(n)^{stat}$, and since in this case the scattering probability is $|\nu_2(n)|^2 \approx \pi n \Gamma^2$, the total probability is straightforwardly obtained. As a result, the expression for I_{dc} reads

$$I_{dc} = \frac{4e}{\hbar} \Delta_0 \Gamma^2 (1 - \sqrt{R}) \langle n \rangle \,, \tag{2.47}$$

which is plotted in Fig. 2.4 as a function of the quality factor.

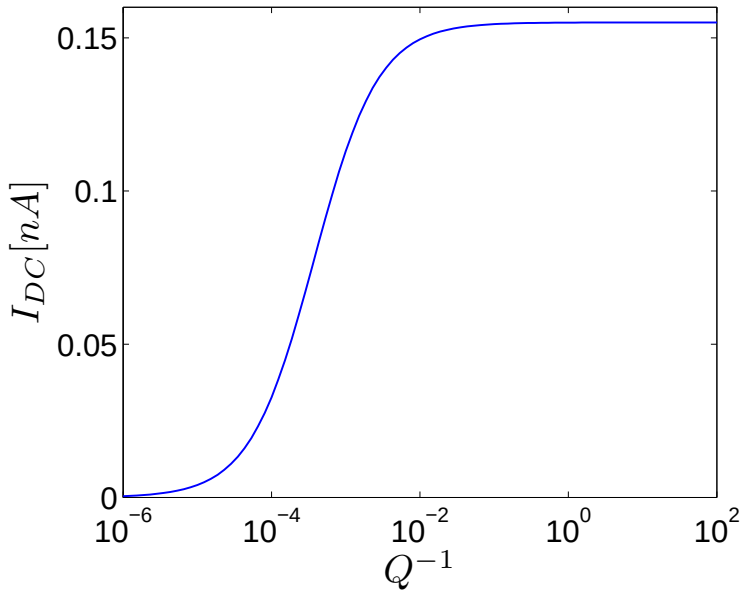

Figure 2.4: DC current as a function of the inverse quality factor in the stationary regime. In the limit of very high quality factor the dc current goes zero. In the opposite limit the dc current approaches a constant value which depends on the external temperature, $I_{dc} \propto n_B$. Here, the system parameters are the same as in Fig. 2.3.

Equation (2.47) shows that the total dc current over the junction is a linear function of the average vibron population in the stationary regime. From Fig. 2.4 we notice that in the limit of small quality factor, *i.e.*, high damping, the dc current saturates to a constant value (0.15 nA). It can be understood by the fact that in this limit the stationary distribution of the vibrational modes is given by the thermal distribution $P_n^{stat} \propto \exp(-n\hbar\omega/k_BT)$, *i.e.* the interactions with the environment are so strong that they always drive the mechanical system into thermal equilibrium, no matter how the inter-Andreev level scattering changes this distribution. As such, $I_{dc} \propto n_B$ in this regime. In the opposite regime, $Q \to \infty$, the dc current goes to zero (within the rotating wave approximation) as expected as this regime corresponds to complete ground state cooling of the mechanical subsystem. If this can be achieved, the probability of Andreev level scattering also goes to zero, $|\nu_2(0)|^2 = 0$, hence the electronic subsystem stays in the lower Andreev branch throughout and the $I_{dc} = 0$.

2.11 Quasiparticle spectrum

At the end of each period, when $\phi(t) = 2\pi$, the bound Andreev levels reach the continuum spectrum and the absorbed vibronic energy is transfered to the quasiparticle states in the leads. This description is based on the following arguments: Firstly, at the edge of each period, the adiabatic condition is no longer valid and the Andreev levels decay into the continuum state. As was highlighted in Ref. [74], this process corresponds to a delocalization in real space and it is the reason for the energy trans-

fer process. Secondly, the orthogonality between Andreev states guarantees that at the beginning of each period the Andreev levels will start again at the lower electronic level [75]. Finally, the analysis showed that the possibility of heating due to the energy transfer process is negligible. Indeed, for a quasiparticle excitation created at the point $\phi(t) = 2\pi$ with characteristic energy $\delta E = \Delta_0(eV/\Delta_0)^{1/3}$ and velocity $v_q p = v_F(eV/\Delta_0)^{1/3}$, where v_F is the Fermi velocity. The traveled distance during one period $T_V = \pi\hbar/eV$ is $\delta x \sim \xi_0(\Delta_0/(eV))^{2/3}$ where $\xi_0 = \hbar v_F/\Delta_0$ is the coherence length of the superconductors. Considering that the size of the junction corresponds to the extension of the Adiabatic Andreev level $\xi = \xi_0(\Delta_0/(eV))^{2/3} \ll \delta x$. Consequently, the quasiparticle has moved away from the junction when the next quasiparticle is created at the boundary edge and the quasiparticle excitation releases energy in the leads which will increase the energy of the thermal bath at the rate $\dot{Q} \ll \Delta_0^2/\hbar(eV/\Delta_0)^{4/3}$. As the energy relaxation process is proportional to the volume of the leads, the above rate is small for heating the leads.

2.12 Final remarks

This chapter summarizes the content of Papers I-II where we have shown that quantum mechanical cooling of a metallic carbon nanotube acting as a nanoelectromechanical Josephson junction is feasible. In the proposed cooling scheme the externally applied magnetic field couples the deflection of the nanowire to the current carried by the Andreev levels. As a consequence, the electronic system can change from one level to the other through the absorption or emission of a quantum of mechanical energy (vibron) given the right experimental parameters. It is also shown that the energy released into the superconducting leads should be experimentally observable through the associated dc current over the junction as a function of the quality factor.

CHAPTER 3

Nonlinear dynamics of a suspended nanowire

In this Chapter we analyze nanoelectromechanical systems (NEMS) as tools for theoretical and experimental studies of nonlinear dynamical systems. As mentioned earlier, NEMS systems are currently considered promising candidates to study nonlinear and complex phenomena due to the inherent properties of these devices, which includes low damping, desired resonant operation, and the presence of nonlinear potential fields [76]. Examples of complex dynamical phenomena in NEMS are numerous and include chaotic behavior [77–80], bifurcation-topology amplification [81], nonlinear switching dynamics [82], and nonlinear frequency pulling [83] to name but a few. For a review on the fundamentals and applications of nonlinearities in NEMS resonators the reader is referred to Refs. [76, 84, 85].

By making use of the potential offered by NEMS resonators, Sonne *et al.* [86] studied the nonlinear dynamics of a suspended carbon nanotube coupled to two voltage-biased superconducting electrodes. In presenting their work, Sonne and collaborators assumed that the nanoelectromechanical junction was subjected to a *homogeneous* magnetic field perpendicular to the axes of the nanowire. For such a system, the authors demonstrated the possibility to pump energy from the electronic subsystem into the mechanical vibrations; they also demonstrated that the system had more than one regime of finite-amplitude stationary nonlinear oscillations. In particular, a region of bistability was found and the authors showed that it should be detected in the corresponding dc Josephson current (see discussion in Ref. [86]).

In this Chapter of the thesis, we consider the same voltage-biased nanoelectromechanical system studied by Sonne and co-workers [86], but now extend the analysis to a case in which the NEMS resonator is subjected to a *nonuniform* magnetic field. As will be discussed in the following sections, inhomogeneity of the field causes the conducting nanoresonator to execute a whirling movement resembling a jump-rope-like motion. The purpose of the subsequent sections is to analyze the time evolution of the amplitude and relative phase of the nanotube whirling motion. We will demonstrate that the coupled amplitude-phase dynamics exhibits different stationary regimes depending on the degree of the magnetic field inhomogeneity: time independent, periodic, and chaotic. This Chapter presents a brief statement of the main points of Paper III.

3.1 System and equations

The diagram in Fig. 3.1 is a schematic illustration of a superconducting hybrid nanostructure, a superconducting-normal-superconducting (S-N-S) nanoelectromechanical

Josephson junction driven by a dc voltage bias V. The junction consists of a metallic carbon nanotube of length L suspended between two voltage-biased superconducting leads. In such a geometry, the nanotube is simultaneously serving as a mechanical resonator and as a weak link between the superconducting electrodes. The phase difference between the weakly coupled leads will be denoted by ϕ and, in accordance with the second Josephson relation, its time evolution is $\phi(t) = \omega_J t$, with $\omega_J = 2eV/\hbar$ the Josephson frequency. In the layout of the system, the NEMS junction is under the influence of an external inhomogeneous magnetic field $\mathbf{H}$, generated by a magnetic force microscope (MFM) cantilever tip in the form of a wedge, parallel to the axis of the nanotube at a distance d. Considering a magnetic field of the form $\mathbf{H} = (0, H_y, H_z)$, a first order Taylor expansion of the magnetic field yields $\mathbf{H} = (0, y\partial_y H_y(x,0,0), H_z(x,0,0) + z\partial_z H_z(x,0,0))$, where $H_z(x,0,0)$ and $\partial_i H_i(x,0,0)$ represent the magnitudes of, respectively, the magnetic field z-component and the magnetic field gradients, both evaluated at the axis of the nanotube. A straightforward calculation from the Maxwell equation $\boldsymbol{\nabla} \cdot \mathbf{H} = 0$, indicates that $\partial_y H_y(x,0,0) = -\partial_z H_z(x,0,0) \equiv -H'_z$. Setting $H_z(x,0,0) \equiv H_z$, the magnetic field reads

$$\mathbf{H} = \left(0, -H'_z y, H_z + H'_z z\right) . \tag{3.1}$$

This field is also obtained from the equation $\mathbf{H} = \boldsymbol{\nabla} \times \mathbf{A}$, with the vector potential $\mathbf{A}$ is given by

$$\mathbf{A} = -\left(\left[H_z + H'_z z\right] y, 0, 0\right) . \tag{3.2}$$

In this scenario, the coupling between the Josephson current and the inhomogeneous magnetic field gives rise to a non-planar whirling displacement of the nanotube due to the Laplace force. As a consequence of the motion in the magnetic field, an electromotive force is induced along the nanomechanical weak-link and its magnitude depends on the rate of change of the nanowire profile in the z-y plane, *i.e.*, the rate of change of the magnetic flux through the circuit. In this description, now, the superconducting phase difference is not only a function of the bias voltage, but also of the nanowire deflection in the z-y plane. We decompose the nanotube motion in this plane into two independent deflections $y(x,t) = u_0(x)a(t)$ and $z(x,t) = u_0(x)b(t)$, where $u_0(x)$ is the normalized and dimensionless profile of the fundamental mode in both directions. Then, the expression for the superconducting phase difference has the form

$$\varphi(t) = \frac{\phi(t)}{2} + \frac{eL}{4\hbar}\left[h_z + h'_z b(t)\right] a(t) . \tag{3.3}$$

The parameters $h_z = \alpha H_z$ and $h'_z = \beta H'_z$ are the renormalized magnetic field and magnetic field gradient in the z-direction calculated at the axis of the tube, respectively, with $\alpha, \beta \sim 1$ correctional factors originating from geometrical considerations. The nanotube mechanics is thus described through the projection amplitudes $a(t)$ and $b(t)$ and for the conjugate variables $\{a(t), p_a(t)\}$ and $\{b(t), p_b(t)\}$ ($p_j(t)$ denoting the generalized momenta) one can formulate the following Hamiltonian function

$$H(p_a, p_b, a, b, t) \;=\; \frac{1}{2m}\left(p_a^2 + p_b^2\right) \;+\; \frac{m\omega^2}{2}\left(a^2 + b^2\right) \;-\; 2D\Delta_0 \cos(\varphi(a,b,t)) , \tag{3.4}$$

where m and ω are the mass and the mechanical eigenfrequency of the nanoresonator, respectively. The last term in Eq. (3.4) corresponds to the Josephson energy

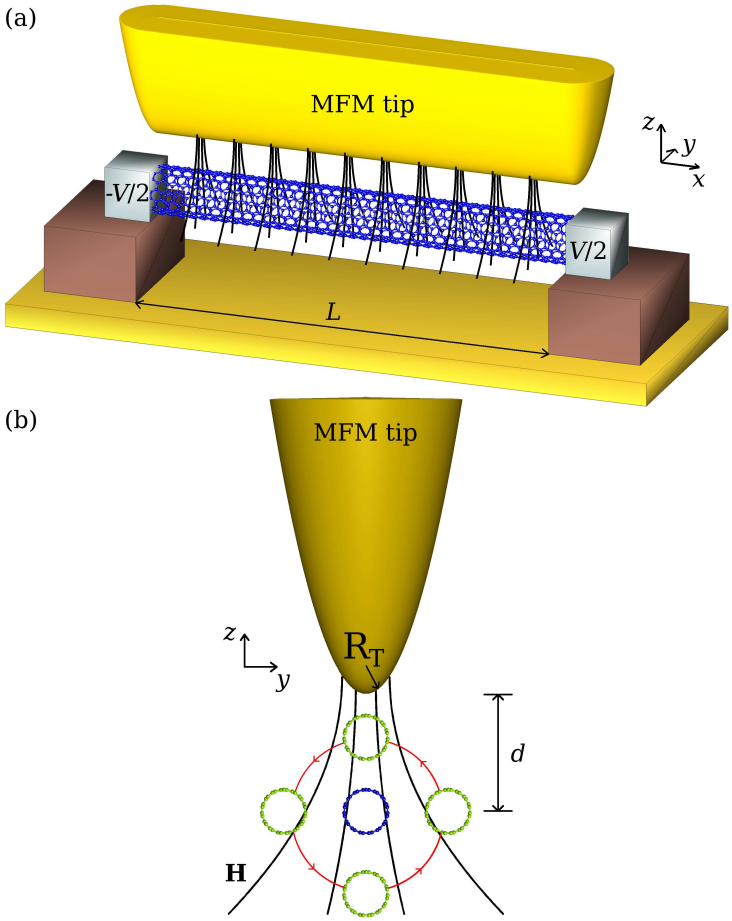

Figure 3.1: (a) Schematic diagram of the voltage-biased S-N-S nanoelectromechanical Josephson junction considered in Paper III. A doubly clamped metallic carbon nanotube suspended over a trench of length L, forms a weak link between two voltage-biased superconducting electrodes. The junction is influenced by an inhomogeneous magnetic field $\mathbf{H}$, generated by a wedge-shaped MFM cantilever tip at a distance d from the nanotube at rest (blue circle). (b) Nanotube displacement (green circles) in the z-y plane induced by a Laplace force. R_T is the curvature radius of the magnetic tip.

$E_J(\varphi(a,b,t))$, with D the transmission coefficient of the junction and Δ_0 the superconducting order parameter. The equations of motion for $a(t)$ and $b(t)$ are then obtained from the Hamilton equations. Written in terms of the dimensionless deflection coordinates

$$\begin{aligned} Y(t) &= \left[eLh_z/4\hbar\right]a(t), \\ Z(t) &= \left[eLh_z/4\hbar\right]b(t), \end{aligned} \tag{3.5}$$

the resulting set of differential equations for the nanotube amplitudes is:

$$\ddot{Y}(\tau) + \tilde{\gamma}\dot{Y}(\tau) + Y(\tau) = -\varepsilon\left[1+\varkappa Z(\tau)\right]\sin\left(\tilde{V}\tau + \left[1+\varkappa Z(\tau)\right]Y(\tau)\right), \tag{3.6}$$

$$\ddot{Z}(\tau) + \tilde{\gamma}\dot{Z}(\tau) + Z(\tau) = -\varepsilon\varkappa Y(\tau)\sin\left(\tilde{V}\tau + \left[1+\varkappa Z(\tau)\right]Y(\tau)\right). \tag{3.7}$$

Here, we have added a dimensionless phenomenological damping coefficient $\tilde{\gamma} = [\gamma/m\omega]$. In these equations $\varepsilon = [2eL^2h_z^2 j_c/m\hbar\omega^2]$ with $j_c = [D\Delta_0 e/2\hbar]$, the critical current through the junction. We also set the timescale to $\tau = \omega t$ and, consequently, $\tilde{V} = [eV/\hbar\omega]$. The parameter

$$\varkappa = \frac{4\hbar}{eLh_zR_T}, \tag{3.8}$$

where $R_T = \left[h_z/h_z'\right]$ denotes the curvature radius of the magnetic cantilever tip, characterizes the degree of inhomogeneity of the magnetic field and will be referred to as the *control parameter*. It turns out that $\varkappa$ determines the dynamical behavior of the system. One can then realize the significance of $\varkappa$ by considering fixed system parameters (L, h_z) and by letting R_T vary. In the limit $R_T \to \infty$, the control parameter vanishes and the equations of motion given by Eqs. (4.13) reduce to the case discused by Sonne *et al.* [86] where the magnetic field is uniform and, therefore, the amplitude of the driving force acting in the Z-direction becomes zero.

3.2 Numerical results and discussion

For a qualitative and quantitative discussion of the dynamic behavior of the nanowire amplitudes, we consider the following system parameters: a carbon nanotube of radius $r = 1$ nm and length $L = 1\,\mu$m [87], superconducting order parameter $\Delta_0 \sim 1$ meV, Josephson critical current $j_c \sim 100$ nA [88], and quality factor $Q \sim 10^3$ [89]. We also assume that $\tilde{\gamma} = 1/Q$, $h_z \sim 40$ mT, $\varepsilon = 0.012$, and R_T is varied from 53 nm to 544 nm. From Eq. (3.8), the control parameter will take values in the interval $0.12 \leq \varkappa \leq 1.25$

Numerical simulations of Eqs. (4.13a) and (4.13b) allow us to study the time average of the nanotube deflection coordinates $Y(\tau)$ and $Z(\tau)$ as functions of the driving voltage $\tilde{V}$. In doing so, one can notice that the system response presents a series of resonance peaks at integer values of the driving voltage, *i.e.*, the amplitude of the nanoresonator is not damped provided the resonant condition is fulfilled: the Josephson frequency matches the mechanical frequency (see Fig. 3.2). This resonant phenomenon was first studied by Sonne *et al.* [86], who attributed a direct resonance at $\tilde{V} = 1$ and a parametric resonance at $\tilde{V} = 2$. Accordingly, the same conclusion can be drawn from the results presented in Fig. 3.2. In the remainder of the chapter we will

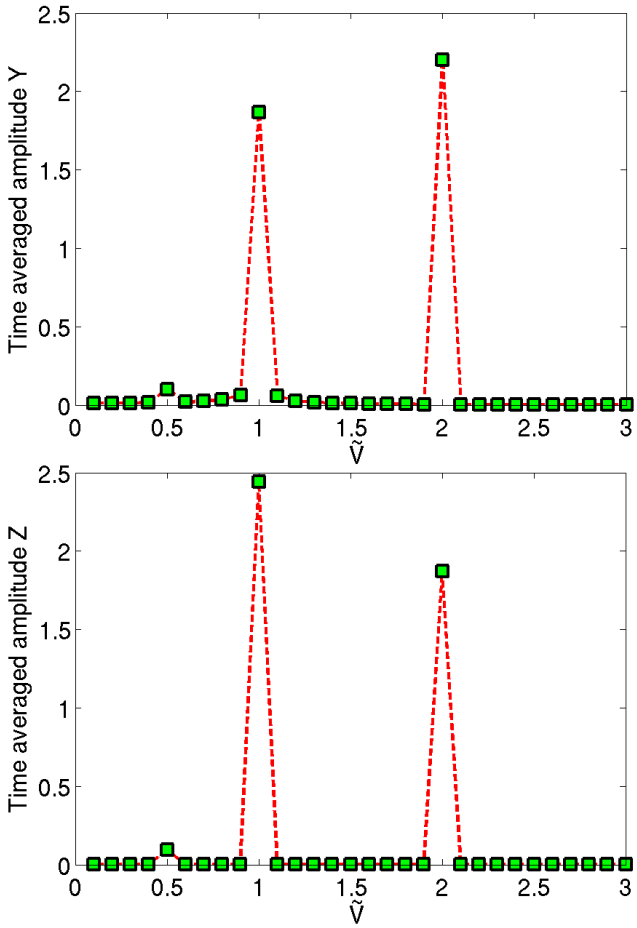

Figure 3.2: Numerical simulations of Eqs. (4.13a) and (4.13b) for the time averaged coordinates Y and Z as function of the driving voltage $\tilde{V}$. The system presents a series of resonance peaks at integer values of the driving voltage and the amplitude of the nanotube is not damped when the Josephson frequency matches the mechanical frequency. Further analysis is performed at parametric resonance $\tilde{V} = 2$. The plots are calculated for $\tilde{\gamma} = 0.001$, $\varepsilon = 0.012$, $\varkappa = 1$ ($L = 1\,\mu$m, $h_z = 40\,$mT, $R_T = 66\,$nm).

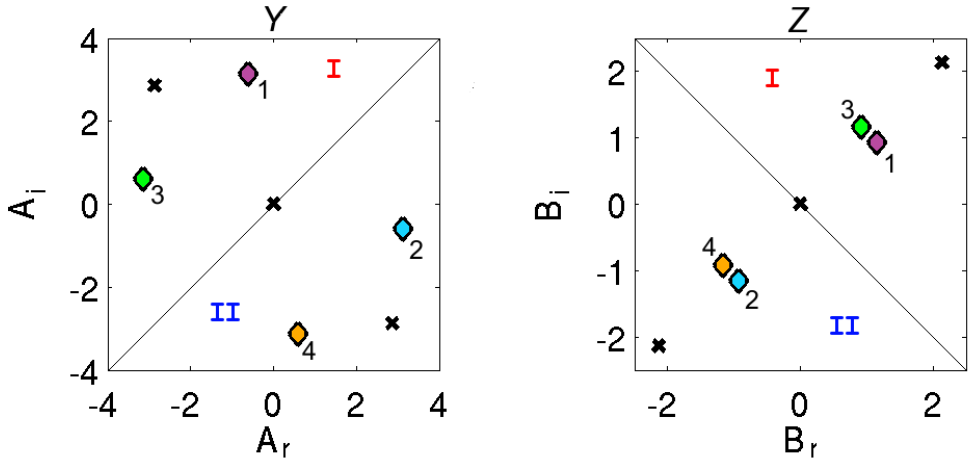

Figure 3.3: Numerical simulations for the stability analysis of Eqs. (3.10). Stable and unstable stationary points are indicated by colored and numbered diamonds (◊) and black crosses (×) respectively. Diamonds of identical color and number indicate the four envelopes of the stable solution $\mathbf{X}_s$, crosses in the same region (I or II) of both phase planes belong to the same unstable solution $\mathbf{X}_u$. The zero solution, $\mathbf{X} \equiv \mathbf{0}$, is unstable. Here, $\tilde{\gamma} = 0.001$, $\varepsilon = 0.012$, $\varkappa = 0.12$ ($L = 1\,\mu$m, $h_z = 40\,$mT, $R_T = 544\,$nm).

be mainly focusing on the parametric regime and take $\tilde{V} = 2$. In this case, the dynamic behavior of the amplitudes can be analized by postulating a solution for both deflection coordinates in the form

$$Y(\tau) = A_r(\tau)\cos(\tau) + A_i(\tau)\sin(\tau)\,, \tag{3.9a}$$
$$Z(\tau) = B_r(\tau)\cos(\tau) + B_i(\tau)\sin(\tau)\,. \tag{3.9b}$$

Here, $A_i; B_i$ and $A_r; B_r$ are the in-phase and quadrature amplitude components of the proposed ansatz for $Y; Z$ given by Eqs. 3.9, respectively. On condition that $\tilde{\gamma}, \varepsilon, \varepsilon\varkappa \ll 1$, the four envelopes in the vector of amplitudes $\mathbf{X} = (A_r(\tau), A_i(\tau), B_r(\tau), B_i(\tau))$ vary slowly in time, *i.e.*, $d\mathbf{X}/d\tau \ll 1$ and, an averaging method [90] can be employed in order to derive the equation of motion for $\mathbf{X}$. By substituting the ansatz provided in Eqs. (3.9) into the system of equations in Eqs. (4.13) and integrating over the fast oscillations one gets

$$\begin{aligned} \frac{dA_r}{d\tau} + \frac{\tilde{\gamma}A_r}{2} &= \frac{\partial \mathcal{G}}{\partial A_i}\,, & \frac{dB_r}{d\tau} + \frac{\tilde{\gamma}B_r}{2} &= \frac{\partial \mathcal{G}}{\partial B_i}\,, \\ \frac{dA_i}{d\tau} + \frac{\tilde{\gamma}A_i}{2} &= -\frac{\partial \mathcal{G}}{\partial A_r}\,, & \frac{dB_i}{d\tau} + \frac{\tilde{\gamma}B_i}{2} &= -\frac{\partial \mathcal{G}}{\partial B_r}\,, \end{aligned} \tag{3.10}$$

where

$$\mathcal{G}(\varkappa) = -\frac{\varepsilon}{2\pi}\int_{-\pi}^{\pi} \cos\big([1 + \varkappa B_r\cos(\Theta) + \varkappa B_i\sin(\Theta)] \times [A_r\cos(\Theta) + A_i\sin(\Theta) + 2\Theta]\big)\, d\Theta\,. \tag{3.11}$$

Here, $\mathcal{G}(\varkappa)$ is the generating Hamiltonian function for Eqs. (3.10).

The study proceeds by performing a stability analysis based on Eqs. (3.10). In general, we shall study solutions of a system of coupled ODEs, $d\mathbf{X}/d\tau = \mathbf{f}(\mathbf{X}, \varkappa)$, and solutions of a system of algebraic equations $\mathbf{0} = \mathbf{f}(\boldsymbol{X}, \varkappa)$. The discussion commences by highlighting the symmetric nature of the stationary solutions for the algebraic system in Eqs. (3.10). For the above considered system parameters with $\varkappa = 0.12\,(R_T = 544\,\mathrm{nm})$, numerical simulations for the slowly-varying envelopes show that the system presents several stationary points. Such qualitative behavior is visualized in the phase space diagrams for the nanotube amplitudes, Y and Z, in Fig. 3.3. There, solutions pictured by colored and numbered diamonds ($\Diamond$) and black crosses ($\times$) correspond to stable and unstable stationary points, respectively. Similarly, the phase portraits are divided in two regions, denoted `I` and `II`, by diagonal symmetry axes. The symmetry axes in the Y and Z coordinates satisfy the relations $A_i - A_r = 0$ and $B_i + B_r = 0$, respectively. From Fig. 3.3 it follows that the presented pattern of solutions has a mirror-image symmetry with respect to the line of symmetry that divides the phase diagrams into regions `I` and `II`, where diamonds of the same color and number represent the four components of a stable computed solution $\mathbf{X}_s$ and crosses in the same region (`I` or `II`) of both phase spaces account for the envelopes of an unstable solution $\mathbf{X}_u$. From a symmetric point of view, the system is characterized by two stable and two unstable (including $\mathbf{X} \equiv \mathbf{0}$) stationary points in each region. However, the dimensionless angular momentum of the nanowire, $\mathbf{L}_x = YdZ/d\tau - ZdY/d\tau$, in both regions is equal in magnitude but opposite in sign.

Table 3.1: Bifurcation pattern in the symmetric regions of solutions `I` and `II` as a function of the control parameter $\varkappa$. Solution $\mathbf{X} \equiv \mathbf{0}$ is included.

$\varkappa$-interval	Number of stable solutions	Number of unstable solutions
$\varkappa \leq 0.120$	2	2
$0.120 < \varkappa \leq 0.125$	3	3
$0.125 < \varkappa \leq 0.140$	1	3

Continuing our exploration, the computed results indicate that the bistable regime is only attained for $\varkappa \leq 0.120$. By letting the control parameter increase further, bistability is abandoned and the number of stationary solutions of Eqs. (3.10) is modified as well as their stability. Indeed, Table 3.1 presents the number of stable and unstable stationary solutions in the interval $0.120 \leq \varkappa \leq 0.140$ in both regions for these equations. As can be seen from the table, the system displays a phenomenon called *branching* or *bifurcation*, which is a distinctive fingerprint of nonlinear dynamical systems [91]. The exhibited branching pattern formation can be described as follows. For $\varkappa \leq 0.120$, bistability is accompanied by two unstable stationary points, one of them corresponds to $\mathbf{X} \equiv \mathbf{0}$ (see Fig. 3.3). Once the control parameter is slightly increased over the threshold value $\varkappa = 0.120$, the nonzero unstable stationary point becomes stable, and simultaneously, two new unstable solutions appear and the system has now three stable and three unstable (including the trivial solution) stationary points. Next, by varying the control parameter in the interval $0.120 \leq \varkappa \leq 0.125$,

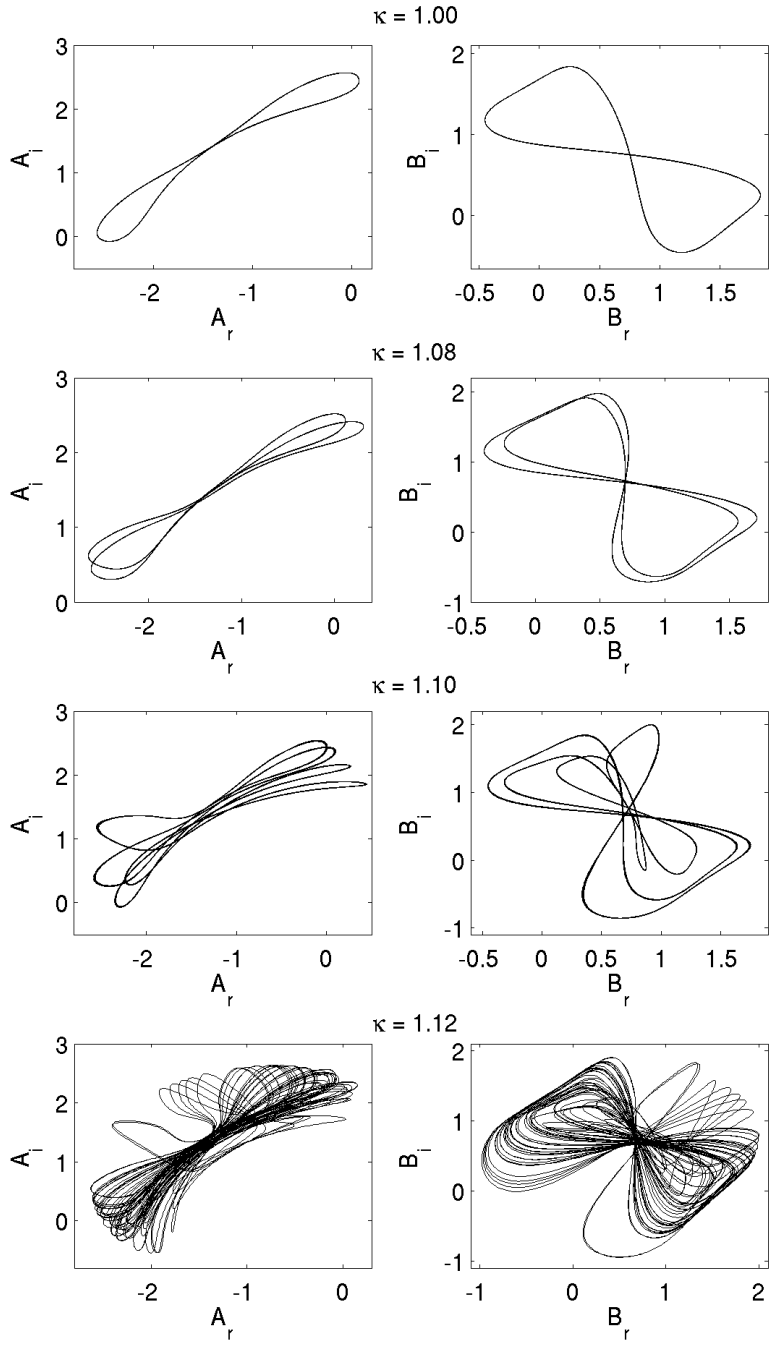

Figure 3.4: Period-doubling bifurcations for different values of the control parameter. Plots are shown for the first symmetry region of both phase spaces. Simulations were obtained for $\tilde{\gamma} = 0.001$, $\varepsilon = 0.012$ ($L = 1\,\mu$m, $h_z = 40\,$mT).

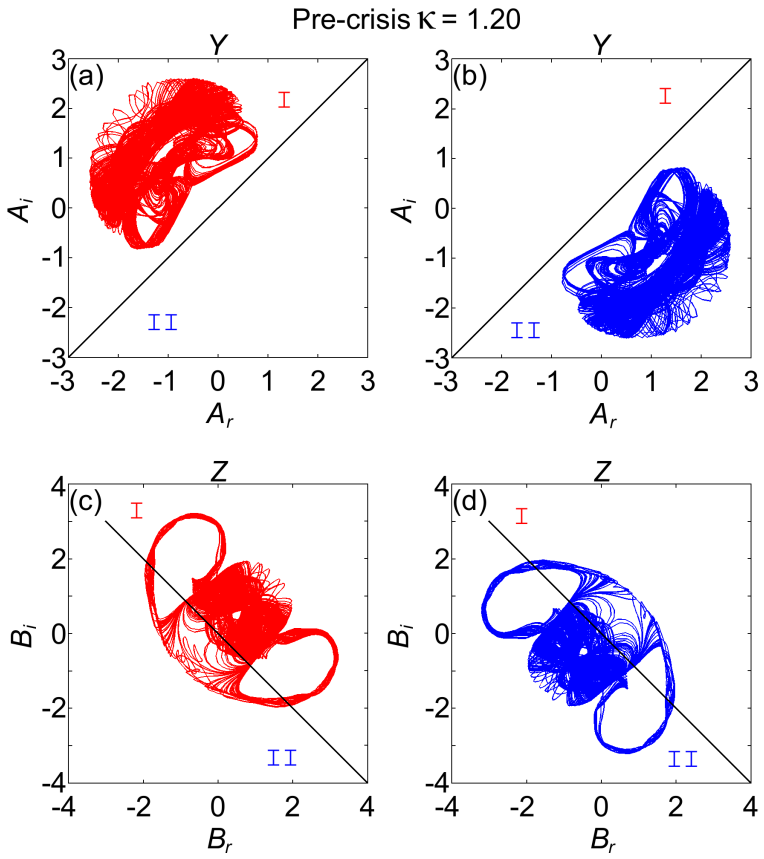

Figure 3.5: Chaotic whirling motion of the suspended carbon nanotube A. In the pre-crisis regime, (a) and (b) depict the two symmetric attractors in the phase spaces for the Y component of the displacement. In (a) red lines indicate the dynamical evolution of a point with initial conditions in the first region of symmetry, region I. Its symmetric dual is shown in (b), where blue lines represent the dynamical flowing of the system for initial conditions in the second region of symmetry. For the Z component of the nanotube motion, (c) and (d) are the symmetric plots for the chaotic attractors. As before, red in (c) and blue lines in (d) account for the evolution of a point with initial conditions in the first and second region of symmetry, respectively. For the plots $\tilde{\gamma} = 0.001$, $\varepsilon = 0.012$, ($L = 1\,\mu$m, $h_z = 40\,$mT).

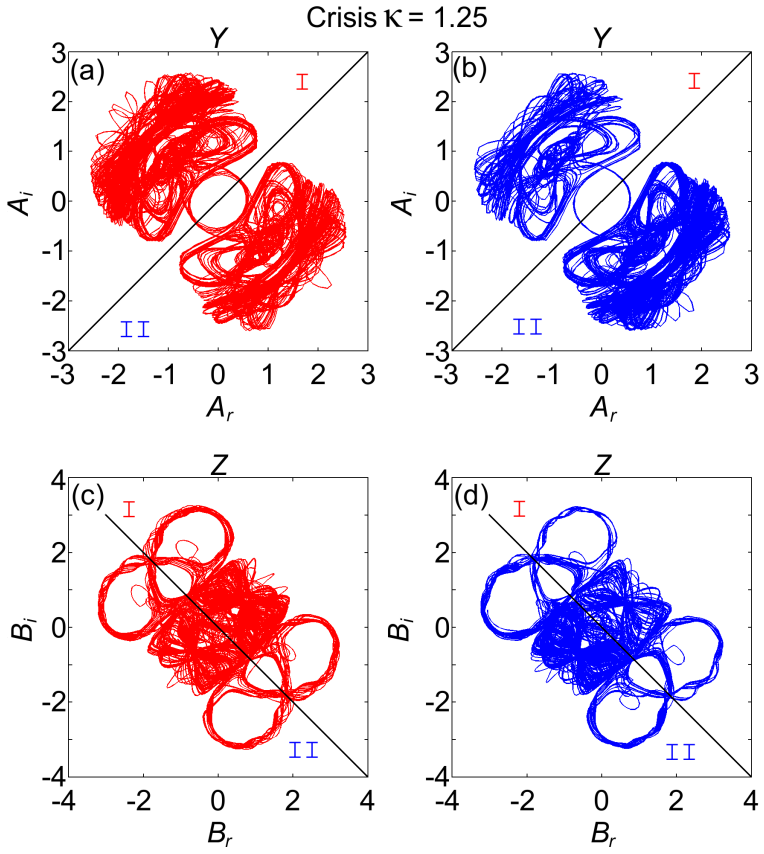

Figure 3.6: Chaotic whirling motion of the suspended carbon nanotube B. In the crisis regime, red lines in (a) and blue lines in (b) show the single chaotic attractor formed by the two symmetric chaotic attractors joined by a periodic orbit on the basin boundary that separates them, the plot is for the dynamics in the Y component. Similarly, for Z-direction, red lines in (c) and blue lines in (d) indicate the attractor merging crisis. For the plots $\tilde{\gamma} = 0.001$, $\varepsilon = 0.012$, ($L = 1\,\mu$m, $h_z = 40\,$mT).

the two original stable points and the two unstable ones move in phase space and approach each other. Finally, when the control parameter ranges from 0.125 to 0.140, the bistable and the created unstable solutions coalesce into two unstable solutions. In this stage, there is only one stable and three unstable stationary points.

It turns out that for $\varkappa > 0.140$, the system leaves the regime of equilibria and enters into the one of periodic solutions. In fact, at the critical control parameter $\varkappa \sim 0.150$, there is an exchange of stability from the unique stable equilibrium to a stable limit cycle. This transformation in phase space is performed through a Poincaré-Andronov-Hopf bifurcation and the computed results show that the stable limit cycle grows in phase space for $0.150 \leq \varkappa \leq 1$. Hereupon, further changes in the control parameter will be reflected in the periodicity of the limit cycle as it can clearly be seen in Fig. 3.4. In this figure, the nanotube dynamics undergoes successive period-doubling cascade bifurcations in the amplitude modulation when varying $\varkappa$. Due to the symmetric character of the solutions, the results are only plotted in region `I`.

Period-doubling bifurcations pave the way for chaotic dynamics [92] and for the control parameter $\varkappa \sim 1.20$; the system is already within this regime. As it is shown in Figs. 3.5(a)-3.5(d), two chaotic attractors coexist and they are symmetric images of each other in the phase space. In Figs. 3.5(a) and 3.5(b), the phase portrait for the slowly varying amplitudes (A_r, A_i) for the Y component of the nanotube displacement is presented. In Fig. 3.5(a), red lines describe the dynamical evolution to the chaotic attractor for a point with initial conditions in the first region of symmetry of the phase space, region `I`. In this case, the attractor and its basin of attraction are completely located in this part of the phase portrait. Its symmetric dual is shown in Fig. 3.5(b), where the chaotic attractor (depicted in blue) and its basin of attraction are found to be in region number `II`; this plot was obtained by a simple study of the evolution of a point with initial conditions in the second region of symmetry, region `II`. Similarly, the qualitative description of the Z component of the nanotube displacement is also analyzed through the phase flow of the slowly varying amplitudes (B_r, B_i). This is shown in Figs. 3.5(c) and 3.5(d), where the symmetric character of the chaotic attractors is noticeable. As before, red lines indicate the dynamics of a point with initial conditions in region `I` and blue ones refer to the complex behavior of a point with initial conditions in the second region of symmetry, `II`. However, there is a difference with respect to the phase portraits for (A_r, A_i). Now, the chaotic attractors are not completely located in each region of symmetry: they cross the symmetry line (that divides the phase portrait into two parts) and enter into the other region, nevertheless, the chaotic attractors and their symmetry are very well defined.

The occurrences of sudden qualitative changes of chaotic attractors, as a parameter of the system is varied, are denoted *crises* [45,46]. In particular, an attractor merging crisis takes place for the studied system when the control parameter reaches the critical value $\varkappa_c \simeq 1.23$. In this phenomenon, the two symmetric attractors simultaneously touch a periodic trajectory or orbit on the basin boundary that separates them and merge together to form a single multipiece chaotic attractor [47,48]. The merging crisis regime can be visualized in Figs. 3.6(a)-3.6(d) where the phase portraits for the nanowire amplitudes suggest that the initially disconnected chaotic attractors, in the pre-crisis state, placed in the symmetric regions `I` and `II` are now joined. Furthermore, the flow diagrams for initial conditions in region `I` (red) and region `II` (blue) indicate that the system dynamically evolves between the two regions, *i.e.*, the flow

lines generated by Eqs. (3.10) and (3.11) are sensitive to the initial values and dense in both regions, where the multipiece single attractor can be readily identified. In order to make the attractor merging crisis clear, we study the dynamics of the system for $\varkappa = 1.25$. The phase portraits for the Y direction have been split for two cases. Red lines in Fig. 3.6(a) account for the dynamics of a point with initial conditions in the first region of symmetry in the pre-crisis regime, while blue lines in Fig. 3.6(b) describe the dynamical evolution of a point initiated in the second region of symmetry, region `II`. In a similar manner, for the Z component, red lines in Fig. 3.6(c) represent the evolution of a point with initial conditions in region `I` and Fig. 3.6(d), the evolution of a point with initial conditions in region `II`.

By increasing further the control parameter, numerical studies indicate that the single attractor formed during the attractor merging crisis is suddenly destroyed (boundary crisis) and then, for parameter values above the crisis, points initialized in the region previously occupied by the former attractor appear to move in the region chaotically, but only for a finite time (chaotic transient) [45, 46]. This phenomenon occurs at $\varkappa \sim 1.6$, however, this value for the control parameter corresponds to a curvature radius of about $R_T = 41$ nm, which is outside the range of curvature radius for MFM tips experimentally reported, $50 - 70\,\mathrm{nm}$ [93]. Due to this fact, the analysis of the transient chaos is not discussed in detail.

3.3 Final remarks

In this chapter we have considered a voltage-biased nanoelectromechanical Josephson junction, where a suspended nanowire is serving as a weak link between two superconducting electrodes, in an inhomogeneous magnetic field. For our case study, we have assumed that the magnetic field is generated by an MFM cantilever tip and the nanowire is in the form of a metallic carbon nanotube. In such a scenario, the inhomogeneity of the field in conjunction with the Josephson current flowing through the tube gives rise to a Laplace force that induces the nanoresonator to perform a whirling movement. We have studied the time evolution of the amplitude and relative phase of this non-planar whirling motion and demonstrated that at the parametric resonance, their coupled dynamics exhibits a rich dynamical behavior characterized by multistability, limit cycles, and chaos. These stationary regimes depend on the degree of the magnetic field inhomogeneity, which in the present case, is related to the curvature radius of the magnetic cantilever tip.

The experimental implementation of the system considered in the article is plausible in light of current state-of-the-art nanofabrication techniques. For instance, Pillet and collaborators designed and constructed a superconducting hybrid nanostructure that comprises a carbon nanotube suspended between two superconductors [94]. Concerning the MFM cantilever tip, the experimental results reported by Matveev and co-workers in Ref. [93] suggest that it is possible to fabricate cantilever tips coated by a magnetic film with a curvature radius in the range of $50 - 70\,\mathrm{nm}$ with maximum magnetic fields in the range of $40 - 80\,\mathrm{mT}$. Due to a growing interest in complex behavior in nanodevices [85], the nonlinear and nonplanar phenomena exhibited by the system studied here have potential applications in signal processing, chaotic encryption, and random number generation [95, 96].

CHAPTER 4

Parametric effects in a shuttle system

In this chapter we investigate theoretically the dynamics of a spatially symmetric shuttle-system subjected to an ac gate voltage. We demonstrate that in such a system parametric excitation gives rise to mechanical vibrations when the frequency of the ac signal is close to the eigenfrequency of the mechanical subsystem. These mechanical oscillations result in a dc shuttle current in a certain direction due to spontaneous symmetry breaking. The direction of the current is defined by the phase shift between the ac gate voltage and the parametrically excited mechanical oscillations. The material discussed in this chapter summarizes the findings discussed in Paper IV.

4.1 System and equations of motion

To describe the new shuttling mechanism, we consider a system schematically depicted in Fig. 4.1 where a single-level quantum dot (D) is connected via elastic links to the left (L) and right (R) electrodes. The characteristic distance between the electrodes and the quantum dot at equilibrium position is d. In this setup the dot is acting as a nano-oscillator, and the deviation of the dot from its equilibrium position is denoted by $x(t)$. Both electrodes are grounded, *i.e.*, $V_L = V_R = 0$, while a signal $V_G = V_G^{st} + V_G^{ac}\cos(\omega_G t)$ is applied to the gate (G). To analyze the electro-mechanical phenomena in such a structure, in the most simplest approximation, we describe the dynamics of the central island by Newton's equation,

$$\ddot{x} + Q^{-1}\omega_0\dot{x} + \omega_0^2 x = \frac{\alpha}{m}e^2 n(t)x. \tag{4.1}$$

Here, m is the mass, ω_0 is the eigenfrequency, and Q is the quality factor of the oscillator. In Eq. (4.1), the parameter $\alpha = [1/(2C^2(0))]\partial^2 C(x)/\partial x^2|_{x=0}$, where $C(x)$ is the effective capacitance of the dot. We consider a symmetric situation $C_T(x) = C_T(-x)$ and one can estimate $\alpha \approx d^{-3}$. Note that in this geometry there is no force acting on the grain if it is in its equilibrium position. The population of the dot $n(t) = 0, 1$ is controlled by the stochastic evolution of the charge.

We focus on the case in which the mechanical vibration frequency of the dot is very low in comparison to the tunneling rates between the quantum dot and electrodes and the electric force is much smaller than the mechanical one, $\alpha e^2/m\omega_0^2 \equiv \epsilon \ll 1$. In such conditions, the force generated by the stochastic variable $n(t)$ can be taken into account only on average by substituting in Eq. (4.1) its mean value $\langle n(t)\rangle = P(t)$. The variable $P(t)$ represents the probability to find one electron in the quantum dot at time t. As a consequence, the electronic state of the central island can be described in

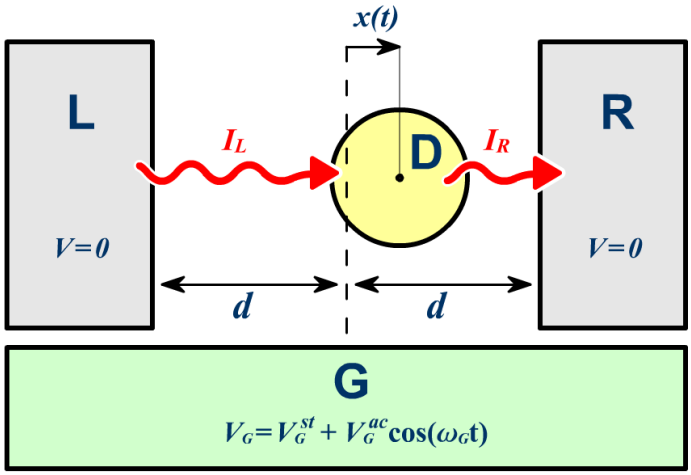

Figure 4.1: Schematic diagram of the three-terminals shuttle device investigated in this work. A quantum dot D can oscillate between two grounded metallic leads L, R. The dot is capacitevely coupled to a gate electrode G, to which a voltage V_G is applied. Electron tunneling takes place between the dot and the leads. I_L and I_R are the currents between the left and right leads L, R and the dot D.

terms of this probability. In accordance with Fig, the time evolution of the probability $P(t)$ is,

$$\begin{aligned}\frac{dP}{dt} &= \left(\frac{dP}{dt}\right)_{in} - \left(\frac{dP}{dt}\right)_{out} \\ &= \left[\left(\frac{dP}{dt}\right)_{in,L} + \left(\frac{dP}{dt}\right)_{in,R}\right] - \left[\left(\frac{dP}{dt}\right)_{out,L} + \left(\frac{dP}{dt}\right)_{out,R}\right].\end{aligned} \tag{4.2}$$

In this case, each independent term in the last equation is defined as [97],

$$\begin{aligned}\left(\frac{dP}{dt}\right)_{in,L} &= (1-P)\Gamma_L(x)f(x,t), \\ \left(\frac{dP}{dt}\right)_{in,R} &= (1-P)\Gamma_R(x)f(x,t), \\ \left(\frac{dP}{dt}\right)_{out,L} &= P\Gamma_L(x)[1-f(x,t)], \\ \left(\frac{dP}{dt}\right)_{out,R} &= P\Gamma_R(x)[1-f(x,t)].\end{aligned} \tag{4.3}$$

Finally, the kinetic equation for the time evolution of the probability P is recast in the following master equation

$$\dot{P} = [\Gamma_L(x) + \Gamma_R(x)](f(x,t) - P)\,. \tag{4.4}$$

Here, the position-dependent tunneling rates between the left/right electrodes and the dot are $\Gamma_{L,R}(x) = \Gamma_0 e^{\mp x/\lambda}$ with λ the tunneling length, $f(x,t) = f(E_D(x,t)) =$

$\left[1+e^{(E_D-\mu)/k_BT}\right]^{-1}$ is the Fermi-Dirac thermal distribution, where μ is the chemical potential of the leads. The energy of the electron inside the dot is $E_D = \varepsilon_\alpha + E_C$, where ε_α is the energy associated to space quantization and $E_C(x,t) = e^2/2C(x) - e\beta V_G(t)$, is the electrostatic energy with $\beta \approx 1$ being the transmission coefficient. Considering $\mu = \varepsilon_\alpha + e^2/2C(0)$ and small displacements of the dot, $x \ll d$, we can rewrite $E_D(x,t) - \mu = -(\alpha/2)e^2 n(t)x^2 - eV_G(t)$.

4.2 DC shutle current

The variation in time of the number of electrons in the leads depends on the applied oscillating voltage $V_G(t)$ and the position of the dot $x(t)$. Therefore, the instantaneous current through the system, averaged over fast fluctuations due to the discrete nature of charge tunneling, is [49, 66]

$$\frac{I_a(t)}{e} = [\Gamma_L(x(t)) - \Gamma_R(x(t))]\{f(x(t),t) - P(t)\}, \tag{4.5}$$

and the dc component of this instantaneous current can be calculated as

$$\begin{aligned}\frac{I_{dc}}{e} &= -\lim_{T\to\infty}\frac{2\Gamma_0}{T}\int_0^T dt\sinh(\frac{x(t)}{\lambda})[f(x(t),t) - P(t)]\,,\\ &= \lim_{T\to\infty}\frac{1}{T\lambda}\int_0^T dt\frac{\dot{x}(t)P(t)}{\cosh^2(x(t)/\lambda)}\,.\end{aligned} \tag{4.6}$$

Here, in writing Eq. (4.6) we use Eq. (4.4). From this expression one can observe that the dc current between the leads is defined by the correlations between the velocity and population of the dot.

4.3 Analysis and discussion

In light of the previous section, in order to study the dc current through the system, one should first analyze the dynamical system defined by Eqs. (4.1) and (4.4). We can perform a perturbative analysis of these equations exploiting the small value of the parameters $\omega_0/\Gamma_0 \backsimeq \omega_G/\Gamma_0 \ll 1$ and $\epsilon, Q^{-1} \ll 1$. In doing so, we can assume

$$P(t) = f(x,t), \tag{4.7}$$

in the leading order of the parameter ω_G/Γ_0. Substituting this relation in Eq. (4.1), we obtained a non-linear and time-dependent equation for x

$$\ddot{x} + Q^{-1}\omega_0\dot{x} + \omega_0^2 x = \epsilon\omega_0^2 f(x,t)x, \tag{4.8}$$

where $f(x,t)$ is a periodic function of time. From this equation, one can find that the mechanical subsystem may experience a parametric instability if $|\omega_G - \omega_0| \ll \omega_0$, when considering the second harmonic term in the Fourier expansion of $f(x,t)$ [98].

Note that Eqs. (4.4) and (4.8) are invariant under the transformation

$$[x(t), P(t)] \to [-x(t), P(t)], \tag{4.9}$$

and it is clear that the only static stationary solution $x(t) = 0$ is invariant under such transformation. If mechanical excitation takes place, it will result in, at least, two different stable periodic (with period $T_G = 2\pi/\omega_G$) solutions:

$$[x_{st}(t), P_{st}(t)] \tag{4.10}$$

$$[\tilde{x}_{st}(t), \tilde{P}_{st}(t)] \equiv [-x_{st}(t), P_{st}(t)] \tag{4.11}$$

From Eq. (4.6), it immediately follows that these two different stationary regimes generate shuttle currents in opposite directions. Which regime arises from the ac-voltage switching will depend on spontaneous forces accompanying transient process. It is worth mentioning that in our considerations we have not taken into account noise forces. Such forces will result in fluctuations of the amplitude and phase around the stationary values [1] and the dc current should be the average over these fluctuations. When fluctuations are much less than the average values, they will modify very little the results discussed here. However, strong fluctuations will lead to transitions between stationary points and, by this, restore the symmetry in the system.

To analyze the regime of parametric excitations one can use the ansatz

$$x(t) = A(t)\cos(\omega_G t + \chi(t))\,, \tag{4.12}$$

where the amplitude $A(t)$ and $\chi(t)$ (the phase shift between the mechanical and gate voltage oscillations) are supposed to be slowly-varying functions of time: $\dot{A}/A, \dot{\chi} \backsimeq \epsilon\omega_G, \omega_G/Q$. It is convenient to introduce the following dimensionless variables: $\tau = \omega_G t$, $\xi = x/\lambda$, and $E = A^2/2\lambda^2$. Then, after substituting the ansatz given by Eq. (4.12) into Eq. (4.8) and averaging over the fast oscillations [99], one obtains the following coupled differential equations for $E(\tau)$ and $\chi(\tau)$,

$$\frac{\partial E}{\partial \tau} = \frac{\partial \mathcal{H}}{\partial \chi} - Q^{-1}E, \tag{4.13a}$$

$$\frac{\partial \chi}{\partial \tau} = -\frac{\partial \mathcal{H}}{\partial E}. \tag{4.13b}$$

Here, $\mathcal{H}$ is the generating Hamiltonian function,

$$\mathcal{H}(E,\chi) \;=\; (\tilde{\omega}_0 \,-\, 1)E \,+\, \frac{\epsilon}{2\eta\pi}\int_{-\pi}^{\pi} d\theta \ln\{1 \,+\, e^{[\eta E\cos^2(\theta)+\nu_{st}+\nu_{ac}\cos(\theta-\chi)]}\}, \tag{4.13c}$$

with $\tilde{\omega}_0 = \omega_0/\omega_G$, $\eta = \alpha e^2\lambda^2/2k_BT$, $\nu_{st} = eV_G^{st}/k_BT$, $\nu_{ac} = eV_G^{ac}/k_BT$. Different stationary oscillation regimes of the dot (labeled by the subscript i) are defined by the different stationary solutions of Eqs. (4.13), *i.e.*, $E_i = \text{const}$, $\chi_i = \text{const}$.

In order to find the dc current corresponding to a given stationary regime of oscillations, $2I_{dc}(E_i,\chi_i) \equiv I_i e\omega_G$, we substitute Eq. (4.7) and Eq. (4.12) into the expression for the dc current given by Eq. (4.6). As a result, it reads

$$I_i = \int_{-\sqrt{2E_i}}^{\sqrt{2E_i}} \frac{d\xi}{\cosh^2(\xi)} \frac{\sinh[b_i\upsilon_i(\xi)\sin(\chi_i)]}{\cosh[a_i(\xi)] + \cosh[b_i\upsilon_i(\xi)\sin(\chi_i)]}, \tag{4.14a}$$

[1] Concerning this issue we would like to emphasise that the amplitude of shot noise fluctuations at the driving frequency ω_G is small due to the fact $\Gamma_0 \gg \omega_G$ and its contributon is negligible.

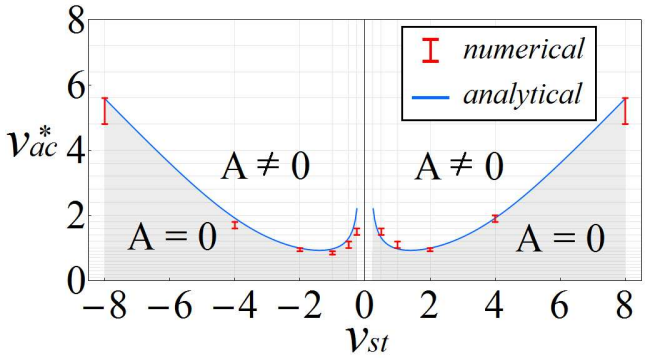

Figure 4.2: Threshold ac voltage ν^*_{ac} as a function of the static dc voltage ν_{st}. Red markers correspond to results obtained from numerical integration of Eqs. (4.1) and (4.4), while blue lines refer to Eq. (4.16). The plot is calculated for a gold quantum dot of radius $r = 4\,\text{nm}$ and mass $m = 5{\times}10^{-21}\,\text{kg}$ with $\omega_0 = 10\,\text{GHz}$, $Q = 1000$, $d \sim 2\,\text{nm}$, $\lambda = 0.1\,\text{nm}$, $\Gamma_0 = 100\,\text{GHz}$, $\omega_G = 10\,\text{GHz}$ and $T = 10\,\text{K}$. Consequently, $\epsilon = 0.1$, $\alpha = 8.37$, $\tilde{\omega} \sim 1$.

with

$$a_i(\xi) = \eta\xi^2 + \nu_{st} + b_i\xi\cos(\chi)\,, \quad b_i = \nu_{ac}/\sqrt{2E_i}. \tag{4.14b}$$

Here, $v_i(\xi)$ is the modulus of the dot velocity as a function of its position given by $v_i(\xi) = \sqrt{2E_i - \xi^2}$. From Eqs. (4.14), we can conclude that the dc current solely exists at non-zero amplitude of oscillation, while its sign (symmetry breaking signature) is controlled by the phase difference χ_i, $\text{sgn}(I_i) \propto \sin(\chi_i)$.

To proceed further, we consider the case of exact resonance,

$$\omega_G = \omega_0\Big\{1 + (\epsilon/4\pi)\int_{-\pi}^{\pi} d\theta[e^{-\nu_{st}} + e^{\nu_{ac}\cos(\theta-\chi)}]^{-1}\Big\}. \tag{4.15}$$

In Eq. (4.15), we have taken into account the renormalization of the frequency due to Coulomb interactions, which is proportional to ϵ. In this situation, the solution $E = 0$ is a stationary point. However, in the frame of a perturbative analysis for small values of E in Eqs. (4.13), one finds that this solution is unstable (parametric mechanical instability) if the condition,

$$\frac{1}{Q\epsilon} \leq \frac{\sin(2\chi_i)}{4\pi}\int_{-\pi}^{\pi} d\theta\cos(2\theta)\tanh(\frac{\nu_{st} + \nu_{ac}\cos(\theta)}{2}), \tag{4.16}$$

is fulfilled. In the above instability criterion, χ_i is defined through the relation,

$$\mathcal{H}(E,\chi_i)/\partial E|_{E=0} = 0\,. \tag{4.17}$$

From Eq. (4.16) one can find that there is a critical amplitude for the ac voltage, $\nu^*_{ac}(\nu_{st})$, above which the system becomes excited. Moreover, if the static voltage tends to zero, $\nu_{st} \to 0$, the critical ac voltage becomes infinite, $\nu^*_{ac} \to \infty$. This threshold ac voltage is shown in Fig. 4.2, where red markers correspond to results obtained from numerical integration of Eqs. (4.1) and (4.4) while blue lines refer to Eq. (4.16).

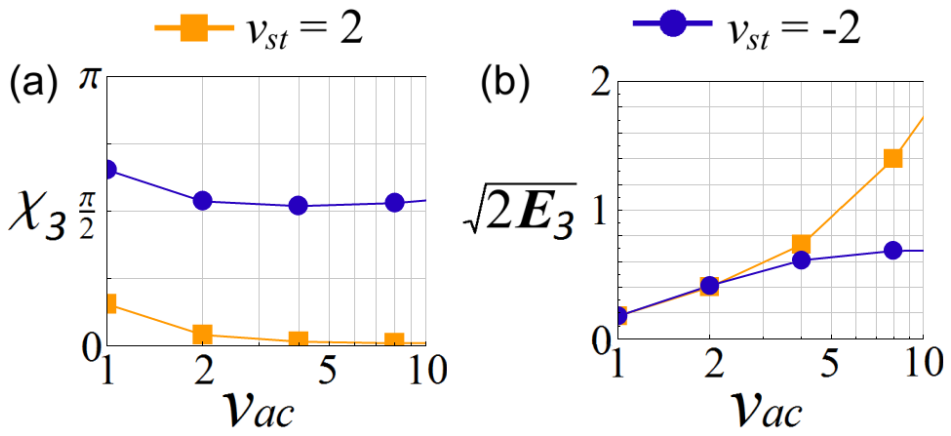

Figure 4.3: Stationary phase (a) and amplitude (b) of the system as a function of the applied static dc voltages $\nu_{st} = 2$ (orange square) and $\nu_{st} = -2$ (blue circles) for different ac voltages ν_{ac}. The phase is almost zero for the positive dc voltage while it is non-vanishing for the negative one. As a result, current transport is more feasible at negative dc voltages (see Eqs. (4.14)). The plot is calculated for $\epsilon = 0.1$, $\alpha = 8.37$, $\tilde{\omega} \sim 1$.

Due to periodicity of the generating Hamiltonian function,

$$\mathcal{H}(E, \chi) = \mathcal{H}(E, \chi + \pi), \tag{4.18}$$

the stationary solutions of Eqs. (4.13) come in pairs, to any solution

$$S_i = \{E_i, \chi_i\}, \tag{4.19}$$

corresponds a conjugated solution

$$\bar{S}_i = \{E_i, \chi_i + \pi\}. \tag{4.20}$$

This fact is a clear manifestation of the symmetry properties of Eqs. (4.4) and (4.8) discussed above. Please notice that the π-dephasing in both solutions is responsible for the sign of the current, *e.g.*, a signature of the symmetry breaking.

In the non-excited regime, *i.e.*, $\nu_{ac}(\nu_{st}) < \nu^*_{ac}(\nu_{st})$, the system defined by Eqs. (4.13) possesses four formal stationary points: $S_1 = \{0, \pi/4\}$, $S_2 = \{0, 3\pi/4\}$ and their conjugates. For $\nu_{st} > 0$, the stationary points $[S_1, \bar{S}_1]$ and $[S_2, \bar{S}_2]$ are stable and unstable, respectively. In the opposite case, $\nu_{st} < 0$, these points exchage stability.

In the regime of oscillations, $\nu_{ac}(\nu_{st}) > \nu^*_{ac}(\nu_{st})$, besides the stationary points $[S_1, \bar{S}_1, S_2, \bar{S}_2]$, two more points, $[S_3 = \{E_3, \chi_3\}, \bar{S}_3 = \{E_3, \chi_3 + \pi\}]$, appear on the phase diagram. The original stationary points S_1, S_2 (and their conjugates) become unstable while the new solutions are stable.

In Fig. 4.3, the phase shift and amplitude of the stable periodic solution $S_3 = \{E_3, \chi_3\}$ are shown as a function of the applied ac voltage (ν_{ac}) for two different static dc voltages: $\nu_{st} = 2$ (blue circles) and $\nu_{st} = -2$ (orange squares). From this graph, one can observe that the phase shift and, as a consequence, the dc current (see Eqs. (4.14)) are

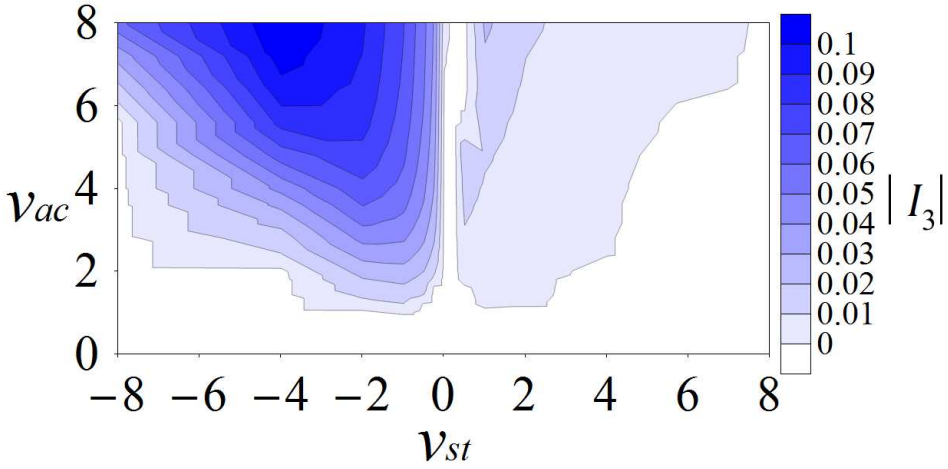

Figure 4.4: Contour plot of the dc current as a function of the applied voltages, $I_3 = I_3(\nu_{st}, \nu_{ac})$. Current through the nanostructure is significant for negative dc voltage values, ν_{st}. In the plot $\epsilon = 0.1$, $\alpha = 8.37$, $\tilde{\omega} = 1$.

almost zero for the positive dc amplitude. However, the plot indicates that the phase is nearly $\chi \sim \pi/2$ and a non-zero dc current is flowing through the nanostructure for the negative dc voltage.

We also investigated the behavior of the dc current as a function of the applied voltages, $I_3 = I_3(\nu_{st}, \nu_{ac})$, and the results are displayed in Fig. 4.4. From the contour map, the assymetric behavior of the dc current with respect to the static dc voltage ν_{st} is evident. Therefore, in the light of results previously discussed, the values of the applied voltages should be choosen in order to maximize the charge transport, *i.e.*, look for a stationary phase $\chi_3 = \pi/2$, this condition is attainable for negative values of ν_{st} as it is shown in Fig. 4.4.

4.4 Final Remarks

To conclude, we have investigated the possibility to generate a shuttle dc current in a completely symmetric single-dot shuttle system. We have demonstrated that, in this scheme, despite the lack of a bias voltage, a shuttle dc current can still be detected. This charge transport is achieved by applying an ac voltage to a gate electrode which controls the electronic population of a metallic island and, in this form, also the stiffness of the resonator. As a result, the metallic dot experiences a parametric mechanical instability at the resonant frequency. We have found that parametric excitation gives rise to two different regimes of sustained mechanical oscillations characterized by the same amplitudes but different phases (they differ by π). These mechanical vibrations result in shuttle transportation of electrons through the nanostructure. In the phenomena under consideration, the shuttle current is controlled by the phase shift and, as a consequence, the two distinct stationary regimes of oscillations generate shuttle currents in opposite directions. Which regime arises from the ac-voltage switching will depend on spontaneous forces accompanying transient process.

CHAPTER 5

Summary

This final Chapter presents brief summaries of the appended papers.

Paper I - Cooling of a suspended nanowire by an ac Josephson current flow

Paper I focuses on the description of a new type of cooling mechanism for a suspended nanowire, in the form of a metallic carbon nanotube, serving as a weak link between two voltage-biased superconducting leads. The possibility to cool the quantized vibrations relies on the transfer of mechanical energy from the flexural vibrations of the nanowire to the electronic quasiparticle in the leads. Cooling is accomplished by the absorption of a quantum of mechanical energy that promotes transitions from the lower to the upper Andreev level. The electromechanical coupling required for the cooling mechanism can be achieved by applying an external magnetic field perpendicular to the axis of the carbon nanotube. In this situation, the mechanical and electronic degrees of freedom are coupled through the Lorentz force. The cooling process is analyzed in the framework of the density matrix formalism and the scattering matrix approach. The study indicates that the nanoresonator can be cooled down to the ground state.

Paper II - Voltage-driven superconducting weak link as a refrigerator for cooling of nanomechanical vibrations

Paper II extends the analysis of Paper I by considering dc current measurements as a probe for the stationary distribution of the population of the vibrational modes. In this paper it is shown that the stationary population of the vibrational modes of the nanowire can be directly measured since it scales linearly with the dc current. This experimental test can be accomplished, for instance, by changing the external pressure of the environment which implies the change of the quality factor of the system. In the limit of high quality factor the dc current is inversely proportional to the quality factor. In the limit of low quality factor the current is independent of the quality factor.

Paper III - Dynamics of a suspended nanowire driven by an ac Josephson current in an inhomogeneous magnetic field

Paper III considers the same voltage-biased nanoelectromechanical system studied in Papers I-II, but now extends the analysis to a case in which the system is subjected to a nonuniform magnetic field. It is assumed that the magnetic field is generated by a magnetic force microscope (MFM) cantilever tip in the form of a wedge. In this situa-

tion, a nonlinear coupling between the Josephson current and the magnetic field generates an oscillatory driving force that induces a nonplanar motion of the nanowire. Numerical studies of the time evolution of the amplitude and relative phase of this whirling motion have demonstrated that at the parametric resonance, their coupled dynamics presents a rich dynamical behavior characterized by: multistability, periodic motion, period doubling, and chaos. These stationary regimes contingent on the degree of the magnetic field inhomogeneity, which in the present case, is related to the curvature radius of the magnetic cantilever tip.

Paper IV - Parametric excitation of a dc shuttle current via spontaneous symmetry breaking

Paper IV analyzes the dynamics of a spatially symmetric shuttle-system, *i.e.*, no applied bias voltage, subjected to an ac gate voltage. In such a system, it has been found that parametric excitation gives rise to mechanical vibrations when the frequency of the ac signal is close to the eigenfrequency of the mechanical subsystem. The most important outcome of this research is that these induced mechanical oscillations result in a dc shuttle current in certain direction due to spontaneous symmetry breaking. In this case, the direction of the current (symmetry breaking) is defined by the phase shift between the ac gate voltage oscillations and the parametrically excited vibrations.

CHAPTER 6

Acknowledgements

I would like to express my gratitude to my advisor Leonid Gorelik for guided me during the years as a graduate student. I also would like to thank my examiner Professor Mats Jonson and Professor Robert Shekhter for all their help. I also would like to give a big thank to Bea, Johanna, Rose-Marie, and Magnus Karlsteen for making my work at the University of Gothenburg so nice. Thank you to all my partners from Chalmers and GU.

A big thank you to the CMT group: Caroline, Gustav, Fabio, Juan, Danko, Hee-Chul, Robert, Yury, Weihua, Daniel, Tora for sharing your experiences. A big thank you to Anders, with whom I have shared office. I really enjoyed our discussions about music, SHP, and Italy. Thank you Tomasz for all the support, patience and friendship. Thank you Aurora for showing us Norway and sharing great moments here in Gothenburg.

I also would like to thank Alessandro Scorrano from La Sapienza University of Rome: Thank you very much for fruitful scientific collaborations.

Life is Sweden has been so enjoyable thanks to Edwin and Brigida and their beautiful family, Nerina and David, Kasper and Vanessa, Don Ener (thank you for your suggestions, support and help), and Jerker. Thank you.

Sharing is caring. A big thank you to: Ale, Vero, William, Job, Eliana, Jadwiga, Tenil, Lilianne, Gaby and her parents, Jorge and family, David, Simon and all members of the REX group.

To my friends in Colombia Néstor, Oscar, Jhon Carlos Molina: Thank you.

I would like to give a big thank you to my family. This thesis is completely dedicated to you. Your support and encouragement were very important in finishing this process.

Gracias especialmente a mi tía Lucila por todo el amor, apoyo, soporte, confianza y fé incondicional. Si existe alguien que en la distancia nos ha acompañado durante todo éste largo trayecto ha sido mi tía Lucila. Gracias por las visitas al ejército, gracias por las vacaciones (especialmente a San Andrés), gracias por todo..... Tía la quiero muchisiisissisisisimo y siempre puede contar con nosotros.

Sin lugar a dudas, ésta tesis es dedicada a mi familiares (Aza - Moreno Castillo). Gracias por todo el apoyo.

Sandra, mi vida entera, mi todo, mi princesita preciosa, mi mundo, la vida misma hecha mujer. Tú eres la fuerza de cada día, eres la prueba más clara del amor de Dios, eres la vida. No existen palabras para expresarte cuánto te amo. Una vida entera no es suficiente para decírtelo. Sin embargo, tú me lo dices con una sonrisa y un beso cada mañana..... Y yo descubro que tú amor es como el oxígeno, que llena de luz mi vida; que me da vida y la felicidad se dibuja en tus ojos. Gracias, Gracias te amo.

Appendix 1: Adiabatic condition for steady level population

In order to avoid Landau-Zener transitions at $\phi(t) = \pi$, the voltage V must be below a certain value which can be estimated using the following arguments: The transition probability from the lower Andreev level to the upper one in the Landau-Zener formalism at the resonant point is

$$P \sim \exp\left[\left(2\Delta_0\sqrt{R}\right)^2/\left(\Delta_0 eV\right)\right]^{-1}, \tag{1}$$

where R is the reflection coefficient due to the impurities in the carbon nanotube and Δ_0 is the superconducting gap. The condition for no transitions from Eq. (1) reads

$$P \sim \exp\left[\left(2\Delta_0\sqrt{R}\right)^2/\left(\Delta_0 eV\right)\right]^{-1} \ll 1\,. \tag{2}$$

The last equation implies that

$$\frac{\left(2\Delta_0\sqrt{R}\right)^2}{\Delta_0 eV} \geq 1\,, \tag{3}$$

and it is possible to conclude that

$$V \leqq V_C = 4\Delta_0 R/e\,, \tag{4}$$

where V_c is the maximum allowed voltage.

Appendix 2: Rotating Wave Approximation

The rotating wave approximation (RWA) was used in Chapter 2.6 to determine the terms in the interaction Hamiltonian that describe Andreev level transitions through the absorption of quanta of mechanical energy. Here, the procedure will be the explained in more detail.
The interaction Hamiltonian of the system is

$$\hat{H}_{int}(t) = \underbrace{\Delta_0 \Phi \sin(\phi(t)/2)}_{g(\phi(t))}[\hat{b}^\dagger + \hat{b}]\hat{\tau}_x \,. \tag{5}$$

By rewriting the Pauli matrix $\hat{\tau}_x$ as

$$\hat{\tau}_x = \left[\begin{pmatrix} 0 & 1 \\ 0 & 0 \end{pmatrix} + \begin{pmatrix} 0 & 0 \\ 1 & 0 \end{pmatrix} \right], \tag{6}$$

the interaction Hamiltonian given by Eq. (5) can be restated as

$$\hat{H}_{int}(t) = g(\phi(t))(\hat{b}^\dagger + \hat{b}) \left[\begin{pmatrix} 0 & 1 \\ 0 & 0 \end{pmatrix} + \begin{pmatrix} 0 & 0 \\ 1 & 0 \end{pmatrix} \right]. \tag{7}$$

By expanding all the products in the last equation it reads

$$\hat{H}_{int}(t) = g(\phi(t)) \left[\hat{b}^\dagger \begin{pmatrix} 0 & 1 \\ 0 & 0 \end{pmatrix} + \hat{b}^\dagger \begin{pmatrix} 0 & 0 \\ 1 & 0 \end{pmatrix} + \hat{b} \begin{pmatrix} 0 & 1 \\ 0 & 0 \end{pmatrix} + \hat{b} \begin{pmatrix} 0 & 0 \\ 1 & 0 \end{pmatrix} \right]. \tag{8}$$

It is possible to elucidate the meaning of each term in Eq. (8) by letting them operate on a general state

$$|\eta\rangle = \begin{pmatrix} 1 \\ 0 \end{pmatrix} |n\rangle + \begin{pmatrix} 0 \\ 1 \end{pmatrix} |m\rangle \,. \tag{9}$$

The first term in the right hand side of Eq. (9) accounts for a state in the upper Andreev level with n vibrons and the second one for a state in the lower Andreev level with m vibrons. Expanding $\hat{H}_{int}(t)|\eta\rangle$ term by term

1.

$$g(\phi(t))\hat{b}^\dagger \begin{pmatrix} 0 & 1 \\ 0 & 0 \end{pmatrix} \left[\begin{pmatrix} 1 \\ 0 \end{pmatrix} |n\rangle + \begin{pmatrix} 0 \\ 1 \end{pmatrix} |m\rangle \right] = g(\phi(t))\sqrt{m+1} \begin{pmatrix} 1 \\ 0 \end{pmatrix} |m+1\rangle \,. \tag{10}$$

The last equation describes the process in which the system is taken from the lower level to the upper level and a vibron is created.

2.
$$g(\phi(t))\hat{b}^\dagger \begin{pmatrix} 0 & 0 \\ 1 & 0 \end{pmatrix} \left[\begin{pmatrix} 1 \\ 0 \end{pmatrix} |n\rangle + \begin{pmatrix} 0 \\ 1 \end{pmatrix} |m\rangle \right] = g(\phi(t))\sqrt{n+1} \begin{pmatrix} 0 \\ 1 \end{pmatrix} |n+1\rangle \,. \quad (11)$$

In this case the system is taken from the upper to the lower level and a vibron is created.

3.
$$g(\phi(t))\hat{b} \begin{pmatrix} 0 & 1 \\ 0 & 0 \end{pmatrix} \left[\begin{pmatrix} 1 \\ 0 \end{pmatrix} |n\rangle + \begin{pmatrix} 0 \\ 1 \end{pmatrix} |m\rangle \right] = g(\phi(t))\sqrt{m} \begin{pmatrix} 1 \\ 0 \end{pmatrix} |m-1\rangle \,. \quad (12)$$

Here, the system is taken from the lower level into the upper level and a vibron is absorbed.

4.
$$g(\phi(t))\hat{b} \begin{pmatrix} 0 & 0 \\ 1 & 0 \end{pmatrix} \left[\begin{pmatrix} 1 \\ 0 \end{pmatrix} |n\rangle + \begin{pmatrix} 0 \\ 1 \end{pmatrix} |m\rangle \right] = g(\phi(t))\sqrt{n} \begin{pmatrix} 0 \\ 1 \end{pmatrix} |n-1\rangle \,. \quad (13)$$

This last term describes the situation when the system is taken from the upper level to the lower level and a vibron is annihilated.

From this analysis it is concluded that the terms describing transitions through the absorption channels are

$$\hat{b}^\dagger \begin{pmatrix} 0 & 0 \\ 1 & 0 \end{pmatrix} \quad \text{and} \quad \hat{b} \begin{pmatrix} 0 & 1 \\ 0 & 0 \end{pmatrix} . \quad (14)$$

After this procedure the interaction Hamiltonian becomes

$$\begin{aligned} \hat{H}_{int}(t) &= g(\phi(t)) \left[\hat{b}^\dagger \begin{pmatrix} 0 & 0 \\ 1 & 0 \end{pmatrix} + \hat{b} \begin{pmatrix} 0 & 1 \\ 0 & 0 \end{pmatrix} \right], \\ &= \Delta_0 \Phi \sin(\phi(t)/2) \begin{pmatrix} 0 & \hat{b} \\ \hat{b}^\dagger & 0 \end{pmatrix} . \end{aligned} \quad (15)$$

Therefore, the total effective Hamiltonian in Eq. (2.17) is

$$\begin{aligned} \hat{H}_{eff}(t) &= \hat{H}_{mech} + \hat{H}_{ele} + \hat{H}_{int}, \\ &= \hbar\omega \hat{b}^\dagger \hat{b} + \Delta_0 \sqrt{1 - D\sin^2(\phi(t)/2)} \begin{pmatrix} 1 & 0 \\ 0 & -1 \end{pmatrix} + \Delta_0 \Phi \sin(\phi(t)/2) \begin{pmatrix} 0 & \hat{b} \\ \hat{b}^\dagger & 0 \end{pmatrix} , \end{aligned} \quad (16)$$

and the Schrödinger equation becomes

$$i\hbar \frac{\partial |\Phi(t)\rangle}{\partial t} = \hat{H}_{eff}(t) |\Phi(t)\rangle \,. \quad (17)$$

If the state of the system $|\Phi(t)\rangle$ is transformed via

$$|\Phi(t)\rangle \rightarrow |\Phi(t)\rangle \exp(-i\omega \hat{b}^\dagger \hat{b}) \,, \quad (18)$$

it is found that the Schrödinger equation, Eq. (17), transforms into

$$i\hbar\frac{\partial|\Phi(t)\rangle}{\partial t} = \hat{\mathcal{H}}_{eff}(t)|\Phi(t)\rangle\,,$$
$$= \begin{pmatrix} E(t) & g(\phi(t))\hat{b}\exp(-i\omega t) \\ g(\phi(t))\hat{b}^{\dagger}\exp(i\omega t) & -E(t) \end{pmatrix}|\Phi(t)\rangle\,. \tag{19}$$

Where $E(t)$ is given by Eq. (2.16). By performing again a new state transformation

$$|\Phi(t)\rangle \rightarrow |\Phi(t)\rangle\exp(-i(\omega/2)\hat{\sigma}_z t)\,, \tag{20}$$

and substituting it in Eq. (19), the Schrödinger equation becomes

$$i\hbar\frac{\partial|\Phi(t)\rangle}{\partial t} = \begin{pmatrix} E(t)-\hbar\omega/2 & \Delta_0\Phi\sin(\phi(t)/2)\hat{b} \\ \Delta_0\Phi\sin(\phi(t)/2)\hat{b}^{\dagger} & -E(t)+\hbar\omega/2 \end{pmatrix}|\Phi(t)\rangle\,. \tag{21}$$

From Eq. (21), the expression for the effective Hamiltonian given in Eq. (2.18) is obtained:

$$\hat{\mathcal{H}}_{eff}(t) = \begin{pmatrix} E(t)-\hbar\omega/2 & \Delta_0\Phi\sin(\phi(t)/2)\hat{b} \\ \Delta_0\Phi\sin(\phi(t)/2)\hat{b}^{\dagger} & -E(t)+\hbar\omega/2 \end{pmatrix}\,. \tag{22}$$

This Hamiltonian was the initial expression for evaluating the probabilities for Andreev levels scattering in Chapter 2.6.

BIBLIOGRAPHY

[1] P. Poncharal, Z. L. Wang, D. Ugarte, and W. A. de Heer, "*Electrostatic deflections and electromechanical resonances of carbon nanotubes*", Science **283**, 1513 (1999).

[2] H. G. Craighead, "*Nanoelectromechanical systems*", Science **290**, 1532 (2000).

[3] V. Sazonova, Y. Yaish, H. Ustunel, D. Roundy, T. A. Arias, and P. McEuen, "*A tunable carbon nanotube electromechanical oscillator*", Nature **432**, 371 (2004).

[4] K. L. Ekinci and M. Roukes, "*Nanoelectromechanical systems*", Rev. Sci. Instrum. **76**, 061101 (2005).

[5] B. Sun and X. H. Huang, "*Mechanical nano-resonators at ultrahigh frequency and their potential applications*", South Africa Journal of Science **104**, 169 (2008).

[6] M. L. Roukes, "*Plenty of room indeed*", Sci. Am. **285**, 42 (2001).

[7] M. L. Roukes, "*Nanoelectromechanical systems face the future*", Phys. World **14**, 25 (2001).

[8] A. Cho, "*Researchers race to put the quantum into mechanics*", Science **299**, 36 (2003).

[9] M. Poot and H. S. van der Zant, "*Mechanical systems in the quantum regime*", Physics Reports **511**, 273 (2012).

[10] A. Cho, "*Faintest Trum Heralds Quantum Machines*", Science **327**, 516 (2010).

[11] M. Roukes, "*Nanoelectromechanical systems face the future*", Physics World **14 (2)**, 25 (2001).

[12] T. Rocheleau, T. Ndukum, C. Macklin, J. B. Hertzberg, A. A. Clerk, and K. C. Schwab, "*Preparation and detection of a mechanical resonator near the ground state of motion*", Nature **463**, 72 (2010).

[13] M. LaHaye, O. Buu, B. Camarota, and K. Schwab, "*Approaching the quantum limit of a nanomechanical resonator*", Science **304**, 74 (2004).

[14] A. J. Legget, "*Testing the limits of quantum mechanics: motivation state of play, prospects*", J. Phys.: Condens. Matter **14**, R415 (2002).

[15] M. P. Blencowe Phys. Rep. **395**, 159 (2004).

[16] K. Schwab and M. Roukes, "*Putting Mechanics into Quantum Mechanics*", Physics Today **58**, No. 7, 36 (2005).

[17] I. Katz, A. Retzker, R. Straub, and R. Lifshitz, "*Signatures for a Classical to Quantum Transition of a Driven Nonlinear Nanomechanical Resonator*", Phys. Rev. Lett. **99**, 040404 (2007).

[18] M. Aspelmeyer, "*The surf is up*", Nature **464**, 685 (2010).

[19] B. Ilic, H. Craighead, S. Krylov, W. Senarathe, C. Ober, and P. Neuzil, "*Attogram detection using nanelectromechanical oscillators*", J. Applied Phys. **95**, 4469 (2004).

[20] H. Mamin and D. Rugar, "*Sub-attonewton force detection at millikelvin temperatures*", Appl. Phys. Lett. **79**, 3358 (2001).

[21] K. Jensen, K. Kim, and A. Zettl, "*An atomic-resolution nanomechanical mass sensor*", Nature Nanotechnology **3**, 533 (2008).

[22] A. N. Cleland, *Foundations of Nanomechanics: From Solid-State Theory to Device Applications*. Springer, Berlin, 2003.

[23] V. B. Braginsky and F. Y. Khalili, *Quantum measurement*. Cambridge University Press, 1992.

[24] K. Likharev, "*Superconducting weak links*", Reviews of Modern Physics **51**, 101 (1979).

[25] M. Tinkham, *Introduction to superconductivity*. Dover Publications, 2004.

[26] H. K. Onnes, "*The resistance of pure mercury at helium temperatures*", Comm. Leiden. **120b** (1911).

[27] J. Bardeen, L. N. Cooper, and J. R. Schriefer, "*Theory of superconductivity*", Phys. Rev. **108**, 1175 (1957).

[28] B. D. Josephson, "*The discovery of tunnelling supercurrents*", Rev. Mod. Phys. **46**, 251 (1974).

[29] A. F. Andreev, "*The thermal conductivity of the intermediate state in superconductors*", Sov. Phys. JETP **19**, 1228 (1964).

[30] A. Andreev, "*Electron spectrum of the intermediate state of superconductors*", Sov. Phys. JETP **22**, 455 (1966).

[31] N. Lundin, *Adiabatic Andreev levels under irradiation-coherent dynamics and dephasing*. PhD thesis, Chalmers University of Technology, 2000.

[32] K. Engström, *Interactions and Interference in Mesoscopic systems: Josephson current through normal quantum dots and Josephson junction arrays*. PhD thesis, Chalmers University of Technology and Göteborg University, 2003.

[33] P. Samuelsson, *Nonequilibrium Effects in Mesoscopic Josephson Junctions*. PhD thesis, Chalmers University of Technology and Göteborg University, 2001.

[34] P. G. de Gennes, *Superconductivity of metals and alloys*. Adison-Wesley Publishing, 1989.

[35] C. W. J. Beenakker, *Transport Phenomena in Mesoscopic Systems*. Springer, Berlin, 1992.

[36] I. Kulik, "*Macroscopic quantization and the proximity effect in S-N-S junctions*", Sov. Phys. JETP **30**, 944 (1970).

[37] P. F. Bagwell, "*Suppression of the Josephson current through a narrow, mesoscopic, semiconductor channel by a single impurity*", Phys. Rev. B **46**, 12573–12586 (1992).

[38] C. W. J. Beenakker and H. van Houten, "*Josephson Current trhough a Superconducting Quantum Point Contact Shorther than the Coherence Length*", Phys. Rev. Lett **66**, 3056 (1991).

[39] G. Wendin and V. S. Shumeiko, "*Josephson transport in complex mesoscopic structures*", Superlattices and Microstructures **20**, 569 (1996).

[40] E. N. Bratus, V. S. Shumeiko, and G. Wendin, "*Scattering theory of superconductive tunneling in quantum junctions*", Low. Temp. Phys. **23**, 181 (1997).

[41] C. W. J. Beenakker, "*Universal limit of critical-current fluctuations in mesoscopic Josephson junctions*", Phys. Rev. Lett. **67**, 3836 (1991).

[42] B. D. Josephson, "*Possible new effects in superconductive tunneling*", Phys. Lett. **1**, 251 (1962).

[43] C. Gragobi, E. Ott, S. Pelikan, and J. A. Yorke, "*Strange attractors that are not chaotic*", Physica D **13**, 261–268 (1984).

[44] Y.-C. Lai and T. Tél, *Transiet Chaos, Complex Dynamics on Finite-Time Scales*. Springer, 2011.

[45] C. Grebogi, E. Ott, and J.Yorke, "*Crises, sudden changes in chaotic attractors, and transient chaos*", Physica D **7**, 181 (1982).

[46] E. O. C. Grebogi and J. Yorke, "*Chaotic Attractors and Crisis*", Phys. Rev. Lett. **48**, 1507 (1982).

[47] K.T.Chau and Z. Wang, *Chaos in Electric Drive Systems: Analysis, Control and Application*. Jhon Wiley & Sons (Asia), 2011.

[48] E. Ott, *Chaos in Dynamical Systems*. Cambridge University Press, 2002.

[49] L. Gorelik, A. Isacsson, M. Voinova, B. Kasemo, R. Shekhter, and M. Jonson, "*Shuttle mechanism for charge transfer in Coulomb blockade nanostructures*", Phys. Rev. Lett. **80**, 4526 (1998).

[50] M. T. Tuominen, R. V. Krotkov, and M. L. Breuer, "*Stepwise and Hysteretic Transport Behavior of an Electromechanical Charge Shuttle*", Phys. Rev. Lett. **83**, 3025–3028 (Oct, 1999).

[51] S. H. M. Persson, L. Olofsson, and L. Gunnarsson, "*A self-assembled single-electron tunneling transistor*", Appl. Phys. Lett. **74**, 2546 (1999).

[52] D. Boese and H. Schoeller, "*Influence of nanomechanical properties on single-electron tunneling: A vibrating single-electron transistor*", Europhys. Lett. **54**, 668 (2001).

[53] Y. Azuma, T. Hatanaka, M. Kanehara, T. Teranishi, S. Chorley, J. Prance, C. G. Smith, and Y. Majima, "*One by one single-electron transport in nanomechanical Coulomb blockade shuttle*", Appl. Phys. Lett. **91**, 053120 (2007).

[54] A. V. Moskalenko, S. N. Gordeev, O. F. Koentjoro, P. R. Raithby, R. W. French, F. Marken, and S. E. Savel'ev, "*Nanomechanical electron shuttle consisting of a gold nanoparticle embedded within the gap between two gold electrodes*", Phys. Rev. B **79**, 241403 (Jun, 2009).

[55] H. Park, J. Park, A. K. Lim, E. H. Anderson, A. P. Alivisotos, and P. L. McEuen, "*Nanomechanical oscillations in a single-C60 transistor*", Nature **407**, 57 (2000).

[56] C. J. Huldt, *Modelling of Molecular-Scale Nanoelectromechanical systems*. PhD thesis, Chalmers University of Technology, 2008.

[57] A. D. Armour and A. MacKinnon, "*Transport via a quantum shuttle*", Phys. Rev. B **66**, 035333 (Jul, 2002).

[58] D. Fedorets, L. Y. Gorelik, R. I. Shekhter, and M. Jonson, "*Quantum Shuttle Phenomena in a Nanoelectromechanical Single-Electron Transistor*", Phys. Rev. Lett. **92**, 166801 (Apr, 2004).

[59] T. Novotný, A. Donarini, and A.-P. Jauho, "*Quantum Shuttle in Phase Space*", Phys. Rev. Lett. **90**, 256801 (Jun, 2003).

[60] T. Novotný, A. Donarini, C. Flindt, and A.-P. Jauho, "*Shot Noise of a Quantum Shuttle*", Phys. Rev. Lett. **92**, 248302 (Jun, 2004).

[61] A. Erbe, C. Weiss, W. Zwerger, and R. H. Blick, "*Nanomechanical Resonator Shuttling Single Electrons at Radio Frequencies*", Phys. Rev. Lett. **87**, 096106 (Aug, 2001).

[62] D. V. Scheible and R. H. Blick, "*Silicon nanopillars for mechanical single-electron transport*", Appl. Phys. Lett. **84**, 4632 (2004).

[63] D. R. Koenig, E. M. Weig, and J. P. Kotthaus, "*Ultrasonically driven nanomechanical single-electrons shuttle*", Nature Nanotech. **3**, 482 (2008).

[64] J. Wiersig, S. Flach, and K.-H. Ahn, "*Discrete breathers in ac-driven nanelectromechanical shuttle arrays*", Appl. Phys. Lett. **93**, 222110 (2008).

[65] N. Nishiguchi, "*Shuttle instability induced by an ac gate in a nanoelectromechanical single-electron transistor*", Phys. Rev. B **78**, 085407 (Aug, 2008).

[66] F. Pistolesi and R. Fazio, "*Charge Shuttle as a Nanomechanical Rectifier*", Phys. Rev. Lett. **94**, 036806 (2005).

[67] F. Pistolesi and R. Fazio, "*Dynamics and current fluctuations in ac-driven charge shuttle*", New J. Phys. **8**, 113 (2006).

[68] E. I. Butikov, "*Parametric Resonance*", Journal Computing in Science and Engineering **1**, 76–83 (1999).

[69] L. Landau and L. E.M, *Mechanics*, vol. 1 of *Course of Theoretical Physics*. Pergamon Press, 1977.

[70] J. J. Sakurai, *Modern Quantum Mechanics*. Addison Wesley Longman, 1994.

[71] J. Kong, E. Yenilmez, T. W. Tombler, W. Kim, H. Dai, R. B. Laughlin, L. Liu, S. Jayanthi, and S. W. Wu, "*Quantum Interference and Ballistic Transmission in Nanotube Electron Waveguides*", Phys. Rev. Lett. **87**, 2538 (2001).

[72] Y. Han, W. Y. Li, L. X. Cao, S. Zhang, B. Xu, and B. Zhao, "*Preparation and superconductivity of iron selenide thin films*", J. Phys.: Condens. Matter **21**, 235702 (2009).

[73] A. K. Hüttel, G. Steele, B. Witkamp, M. Poot, L. P. Kouwenhoven, and H. S. J. van der Zant, "*Carbon Nanotubes as Ultrahigh Quality Factor Mechanical Resonators*", Nano Lett. **9**, 2547 (2009).

[74] L. Y. Gorelik, N. I. Lundin, V. S. Shumeiko, R. I. Shekhter, and M. Jonson, "*Superconducting Single-Mode Contact as a Microwave-Activated Quantum Interferometer*", Phys. Rev. Lett. **81**, 2538 (1998).

[75] N. I. Lundin, "*Dynamics of adiabatic Andreev levels in microwave-irradiated superconducting single-mode contacts*", Phys. Rev. B **61**, 9101 (2000).

[76] J. F. Rhoads, S. W. Shaw, and K. L. Turner, "*Nonlinear Dynamics and Its Applications in Micro- and Nanoresonators*", J. Dyn. Sys., Meas., Control **132**, 034001 (2010).

[77] R. B. Karabalin, M. C. Cross, and M. L. Roukes, "*Nonlinear dynamics and chaos in two coupled nanomechanical resonators*", Phys. Rev. B **79**, 165309 (Apr, 2009).

[78] F. N. Mayoof and M. A. Hawwa, "*Chaotic behavior of a curved carbon nanotube under harmonic excitation*", Chaos, Solitons and Fractals **42**, 1860 (2009).

[79] M. A. Hawwa and H. M. Al-Qahtani, "*Nonlinear oscillations of a double-walled carbon nanotube*", Computational Material Science **48**, 140 (2010).

[80] E. Kenig, Y. A. Tsarin, and R. Lifshitz, "*Homoclinic orbits and chaos in a pair of parametrically driven coupled nonlinear resonators*", Phys. Rev. E **84**, 016212 (2011).

[81] R. B. Karabalin, R. Lifshitz, M. C. Cross, M. H. Matheny, S. C. Masmanidis, and M. L. Roukes, "*Signal Amplification by Sensitive Control of Bifurcation Topology*", Phys. Rev. Lett. **106**, 094102 (2011).

[82] Q. P. Unterreithmeier, T. Faust, and J. P. Kotthaus, "*Nonlinear switching dynamics in a nanomechanical resonator*", Phys. Rev. B **81**, 241405 (2010).

[83] M. C. Cross, A. Zumdieck, R. Lifshitz, and J. L. Rogers, "*Synchronization by Nonlinear Frequency Pulling*", Phys. Rev. Lett. **93**, 224101 (2004).

[84] R. Lifshitz and M. Cross, *Reviews of Nonlinear Dynamics and Complexity*, ch. 1, pp. 1–52. Wiley-VCH Verlag GmbH & Co. KGaA, Weinheim, Germany, 2009.

[85] M. G. E. da Luz and C. Anteneodo, "*Nonlinear dynamics in meso and nano scales: fundamental aspects and applications*", Phi. Trans. R. Soc. A **369**, 245 (2011).

[86] G. Sonne, R. I. Shekhter, L. Y. Gorelik, S. I. Kulinich, and M. Jonson, "*Superconducting pumping of nanomechanical vibrations*", Phys. Rev. B **78**, 144501 (2008).

[87] R. Saito, G. Dresselhaus, and M. Dresselhaus, *Physical Properties of Carbon Nanotubes*. Imperial College Press, 1998.

[88] A. Y. Kasumov, R. Deblock, M. Kociak, H. B. B. Reulet, I. Khodos, Y. Gorbatov, V.T.Volkov, C.Journet, and M.Bughard, "*Supercurrents Through Single-Walled Carbon Nanotubes*", Science **284**, 1508 (1999).

[89] B. Witkamp, M.Poot, and H. van der Zant Nano Lett. **6**, 2904 (2006).

[90] A. H. Nayfeh, *Perturbation Methods*. Wiley, John & Sons, Incorporated, August 2000.

[91] R. Seidel, *Practical bifurcation and stability analysis : From equilibrium to chaos*. Springer-Verlag, New York, 1994.

[92] J. Argyris, G. Faust, and M. Haase, "*Routes to chaos and turbulence. A computational introduction*", Phi. Trans. R. Soc. Lond. A **344**, 207 (1993).

[93] V. N. Matveev, V. I. Levashov, V. T. Volkov, O. V. Kokonenko, A. V. Chernyh, M. A. Knjazev, and V. A. Tulin, "*Fabrication and use of a nanoscale Hall probe for measurements of the magnetic field induced for MFM tips*", Nanotechnology **19**, 475502 (2008).

[94] J. Pillet, C. Quay, P.Morfin, C.Bena, A. Yeyati, and P. Joyez, "*Andreev bound states in supercurrent-carrying carbon nanotubes revealed*", Nature Phys. **6**, 965 (2010).

[95] W. G. Conley, A. Raman, C. M. Krousgrill, and S. Mohammadi, "*Nonlinear and Nonplanar Dynamics of Suspended Nanotube and Nanowire Resonators*", Nano Lett. **8**, 1590 (2008).

[96] Q. Chen, L. Huang, Y. C. Lai, C. Gragobi, and D. Dietz, "*Extensively Chaotic Motion in Electrostatically Driven Nanowires and Applications*", Nano Lett. **10**, 406 (2010).

[97] G. L. Ingold and Y. Nazarov, *Charge tunneling rates in ultrasmall junctions*. H. Grabert and M.H. Devoret (ed.), "Single Charge Tunneling - Coulomb Blockade Phenomena in Nanostructures" NATO ASI series, Vol. B294, pages 21-107, Plenum Press, New York, 1992.

[98] D. Midtvedt, Y. Tarakanov, and J. Kinaret, "*Parametric Resonance in Nanoelectromechanical Single Electron Transistor*", Nano Lett. **11**, 1439 (2011).

[99] A. H. Nayfeh and D. T. Mook, *Nonlinear Oscilations*. Wiley-VCH, 2004.